AN EXPERIMENTAL STUDY OF COMPRESSIONAL HYDROMAGNETIC WAVES

Thesis by

D. Gary Swanson

In Partial Fulfillment of the Requirements

For the Degree of

Doctor of Philosophy

California Institute of Technology

Pasadena, California

1963

ACKNOWLEDGEMENT

The author wishes to express his deep appreciation to Professor Roy W. Gould for his advice, interest and encouragement throughout this investigation. Mr. Robert Hertel is also thanked for his help in the design and construction of the equipment, and thanks go to Mr. George Lieberman for his help in some phases of design of the apparatus and in the theory of the plasma-filled waveguide. Thanks are also extended to Mr. Andrew Dienes, Mr. Eric Gelin and Mr. Noel Payne who aided in the construction of the equipment and to Mrs. Ruth Stratton who prepared the manuscript.

This investigation was conducted under the auspices of the U.S. Air Force Office of Scientific Research.

ABSTRACT

An experiment is described in which a compressional hydromagnetic wave is observed in a hydrogen plasma-filled waveguide. The theory of a cool, partially ionized, resistive plasma in a magnetic field is described briefly and expressions are derived for the dispersion relation and transfer function which include both the propagation and attenuation constants as a function of frequency. Measurements of the cutoff frequency are presented which verify its linear dependence on the magnetic field, and they show good agreement with theory on the variation with the ion mass density. The impulse response of the plasma is studied, transformed into the frequency domain, and quantitative comparisons are made with the theoretical transfer function to determine the degree of ionization, the resistivity, and the ion-neutral collision frequency.

Results indicate that the degree of ionization varies over a range from 75% to 45% when the initial density changes from $1.3 \cdot 10^{21}$ to $1.4 \cdot 10^{22}$ atoms/m^3. The measured resistivity appears to increase with the magnetic field, with the mean value corresponding to a temperature of the order of $5 \cdot 10^3$ ^oK . The average value of the product of the charge exchange cross section and the neutral thermal speed is found to be approximately $(5.5 \pm 1.3) \cdot 10^{-15}$ m^3/sec.

EXPERIMENTAL STUDY OF COMPRESSIONAL

HYDROMAGNETIC WAVES

Table of Contents

INTRODUCTION

The first description of hydromagnetic waves was given by Hannes Alfvén (1) in 1942, when he proposed that they might account for the existence of sunspots. This original work was followed by treatments of these waves by Walén (2), Aström (3), and Herlofson (4). Since then a considerable literature has been developed on the theory of these waves (see Ph.D. Thesis of A. DeSilva (5) for Bibliography and review of literature), but little has been done experimentally until recent years. The reason for this is that for laboratory plasmas with practical magnetic fields very high conductivities were necessary to obtain a wave that was not highly damped. Initially, experiments were performed in the liquid metals mercury and sodium by Lundquist (6) and Lehnert (7). These experiments detected the wave, but the damping was very high, as expected.

As plasma technology advanced rapidly, it became possible in recent years to observe these hydromagnetic waves in a gaseous plasma. Although most laboratory plasmas do not have a high conductivity, the greatly increased wave velocity reduces the attenuation, since the attenuation per wavelength is approximately inversely proportional to both the conductivity and the Alfvén speed, with the result that dissipation is much less than in the liquid metals. Reports of the actual experimental observation of hydromagnetic waves in a plasma appeared almost simultaneously in 1959 by Allen et al (8) and Jephcott (9). A more detailed study was reported by Wilcox et al (10) in 1960 of the work begun by Allen. A study of the ion-cyclotron resonance effect was reported by Stix (11).

All of the above-mentioned experimental observations of hydromagnetic waves were of the torsional type wave in which the experiments were done in cylindrical geometry, and the wave magnetic field perturbed the axial static magnetic field in a torsional manner. Another type of wave exists which is compressional by nature, in that the wave magnetic field tends to alternately compress and expand the static axial field. Whereas the former mode has a resonance at the ion-cyclotron frequency, so that the experiments on that mode always involve wave frequencies less than or equal to the ion-cyclotron frequency, the compressional mode has its resonance at the electron-cyclotron frequency and has a waveguide cutoff frequency determined by the Alfvén speed and the geometry. Experimental observations of this mode have recently been reported by the author and R. W. Gould (12) and by Jephcott (13). In the former experiment a hydrogen plasma was employed and a band of frequencies from below the cutoff frequency up to and beyond the ion-cyclotron frequency was studied. The investigation reported herein is an extension of that work. The latter experiment was done in an argon plasma, and the wave frequencies were always above the ion-cyclotron frequency.

This study was originally undertaken first to observe the compressional wave, and then to determine quantatively the adequacy of a three-fluid theoretical model of plasma in describing the propagation of this wave. The model of a cold plasma in a strong magnetic field with electron-ion and ion-neutral collision effects included is first developed with the plasma represented by a generalized dielectric tensor. Maxwell's equations are then solved using the non-diagonal generalized

dielectric tensor, and the dispersion relation is calculated finally with a high-speed digital computer.

The experimental apparatus is very similar to that used by Wilcox et al (10), except that the wave excitation mechanism is modified to generate the compressional mode. Measurements have been made of the variation of the cutoff frequency, which is proportional to the Alfvén speed, with magnetic field and initial gas density. We depend on the shot-to-shot reproducibility of the system to interpret these results, which limits the accuracy of the experiment. Also, the impulse response of the system has been studied, and this gives, on a single shot, information on the dispersion relation over a frequency band which extends from below the cutoff frequency to beyond the ion-cyclotron frequency. This method involves taking the Fourier transform of the impulse response, which gives the experimental transfer function, and fitting it to a theoretical transfer function. The curve fitting is used to determine the degree of ionization, the resistivity, and the ion-neutral collision frequency.

In addition, measurements of the radial distribution of the wave field have been made, and observations of higher modes are discussed.

CHAPTER I

THEORETICAL MODEL FOR THE PLASMA

As a model for the plasma in a plasma-filled waveguide we shall assume that the plasma is:

1. Uniform $(\nabla N = 0)$
2. Neutral $(N_i = N_e = N)$
3. Singly ionized
4. Axially magnetized $(\underset{\sim}{B}_o = B_o \underset{\sim}{e}_z)$
5. Partially ionized $(N = \gamma N_o,\ 0 < \gamma \leq 1)$
6. Cool, i.e.,
   a) we neglect pressure and other explicit temperature effects, such as viscosity, etc;
   b) we include the temperature only through collisions.

Condition 6a is appropriate only when the magnetic pressure $p_m = B^2/2\mu_o$ is much greater than NkT, i.e., when the Alfvén speed is much greater than the ion thermal speed. Utilizing condition 6a we can use the second moments of the Boltzmann equations for the electrons, ions and neutrals and need not consider any higher moments. Hence we may write for the electrons

$$N_e m_e \left[\frac{\partial \underset{\sim}{v}_e}{\partial t} + \underset{\sim}{v}_e \cdot \nabla \underset{\sim}{v}_e \right] = - N_e e \left[\underset{\sim}{E} + \underset{\sim}{v}_e \times \underset{\sim}{B} \right] + \underset{\sim}{P}^{ei} + \underset{\sim}{P}^{en} \qquad (1.1a)$$

where the $\underset{\sim}{P}^{ij}$ represents the momentum per unit volume per second transferred from the j^{th} to the i^{th} species of the plasma due to collisions. The subscripts

$$e,\ i,\ n$$

refer to electrons, ions and neutrals, respectively. We can also write

immediately for the ions

$$N_i m_i \left[\frac{\partial \underset{\sim}{v}_i}{\partial t} + \underset{\sim}{v}_i \cdot \nabla \underset{\sim}{v}_i \right] = N_i e(\underset{\sim}{E} + \underset{\sim}{v}_i \times \underset{\sim}{B}) + \underset{\sim}{P}^{ie} + \underset{\sim}{P}^{in} \qquad (1.1b)$$

and for the neutrals

$$N_n m_n \left[\frac{\partial \underset{\sim}{v}_n}{\partial t} + \underset{\sim}{v}_n \cdot \nabla \underset{\sim}{v}_n \right] = \underset{\sim}{P}^{ne} + \underset{\sim}{P}^{ni} \quad . \qquad (1.1c)$$

We shall assume now that the electron-neutral momentum transfer cross-section is much smaller than the ion-neutral cross-section and neglect $\underset{\sim}{P}^{en}$ and $\underset{\sim}{P}^{ne}$. We shall also assume $e^{i\omega t}$ time dependence and consider small perturbations from the steady state, where $\underset{\sim}{v}_o = \underset{\sim}{E}_o = 0$ but that $\underset{\sim}{B}$ has a steady value $B_o \underset{\sim}{e}_z$ in the z direction.

With the above assumptions, we may write the linearized Boltzmann equations as

$$i\omega N_e m_e \underset{\sim}{v}_e = - N_e e(\underset{\sim}{E} + \underset{\sim}{v}_e \times \underset{\sim}{B}_o) + \underset{\sim}{P}^{ei} \qquad (1.2a)$$

$$i\omega N_i m_i \underset{\sim}{v}_i = N_i e(\underset{\sim}{E} + \underset{\sim}{v}_i \times \underset{\sim}{B}_o) + \underset{\sim}{P}^{ie} + \underset{\sim}{P}^{in} \qquad (1.2b)$$

and

$$i\omega N_n m_n \underset{\sim}{v}_n = \underset{\sim}{P}^{ni} \quad . \qquad (1.2c)$$

We shall consider 1.2c first. In order to obtain an expression for $\underset{\sim}{P}^{ni}$ we note that the charge-exchange cross-section dominates the other cross-sections for ion-neutral momentum transfer (5). In a charge exchange collision, the particles usually pass far enough apart that relatively little momentum is transferred except that the ion and

neutral interchange roles. Thus the collision is effectively a head-on collision, and in such a case the momentum gained by a neutral per collision is very nearly $m_n(\underset{\sim}{v}_i - \underset{\sim}{v}_n)$ (since $m_i \approx m_n$) . The number of such collisions per unit volume per second is just the neutral particle density times the ion-neutral collision frequency ν . In this case the expression for P^{ni} is given by

$$\underset{\sim}{P}^{ni} = m_n(\underset{\sim}{v}_i - \underset{\sim}{v}_n)N_n\nu \ . \tag{1.3}$$

Substituting into 1.2c we get

$$i\omega N_n m_n \underset{\sim}{v}_n = m_n(\underset{\sim}{v}_i - \underset{\sim}{v}_n)N_n\nu \ . \tag{1.4}$$

If we now solve 1.4 for $\underset{\sim}{v}_n$, where we let $\tau = 1/\nu$ we obtain

$$\underset{\sim}{v}_n = \frac{\underset{\sim}{v}_i}{1 + i\omega\tau} \tag{1.5}$$

and now if we put this into 1.3 we have

$$\underset{\sim}{P}^{ni} = \frac{i\omega \underset{\sim}{v}_i m_n N_n}{1 + i\omega\tau} \approx \frac{i\omega \underset{\sim}{v}_i m_i N_n}{1 + i\omega\tau} \ . \tag{1.6}$$

Now we note that always

$$\underset{\sim}{P}^{ij} = - \underset{\sim}{P}^{ji} \tag{1.7}$$

so that we may now return to equation 1.2b and obtain

$$i\omega \underset{\sim}{v}_i N_i m_i \left[1 + \frac{N_n}{N_i(1 + i\omega\tau)}\right] = Ne(\underset{\sim}{E} + \underset{\sim}{v}_i \times \underset{\sim}{B}_o) + \underset{\sim}{P}^{ie} \ . \tag{1.8}$$

We may now define a new pseudo ion mass μ so that

$$\mu \equiv m_i \left[1 + \frac{N_n}{N_i(1 + i\omega\tau)} \right] . \tag{1.9}$$

If we now assume that γ is the percent ionization and that

$$N = N_i = N_e = \gamma N_o \tag{1.10a}$$

and

$$N_n = (1 - \gamma)N_o \tag{1.10b}$$

we may rewrite 1.9 as

$$\mu = m_i \left(\frac{\frac{1}{\gamma} + i\omega\tau}{1 + i\omega\tau} \right)$$

$$= m_i \left(\frac{\frac{\nu}{\gamma} + i\omega}{\nu + i\omega} \right) . \tag{1.11}$$

From this expression it is clear that if $\omega \gg \nu/\gamma$ then $\mu \to m_i$; and the neutrals may be neglected. On the other hand, if $\nu \gg \omega$, $\mu \to m_i/\gamma$ so that the ions look heavier. This is due to the fact that then N_o ion masses in the system are being carried along by the disturbance but only γN_o charges are carrying them along, so each charged particle appears to have an artificially low e/m ratio. Note that μ contains all the information about the neutrals.

If we now use the definition 1.9 in 1.8 we get

$$i\omega \underset{\sim}{v}_i = \frac{e}{\mu} (\underset{\sim}{E} + \underset{\sim}{v}_i \times \underset{\sim}{B}_o) + \frac{\underset{\sim}{P}^{ie}}{N\mu} \tag{1.12a}$$

and rewriting 1.2a in a similar form

$$i\omega \underset{\sim}{v}_e = -\frac{e}{m_e}(\underset{\sim}{E} + \underset{\sim}{v}_e \times \underset{\sim}{B}_o) + \frac{\underset{\sim}{P}^{ei}}{Nm_e} \quad . \tag{1.12b}$$

When we now consider the electron-ion collisions, we shall assume the momentum transfer to be proportional to the relative average velocities of the electrons and ions and to the ion density, or simply to the current density. We will define the constant of proportionality by

$$\eta \underset{\sim}{J} \equiv \frac{\underset{\sim}{P}^{ei}}{Ne} = -\frac{\underset{\sim}{P}^{ie}}{Ne} \tag{1.13}$$

where

$$\underset{\sim}{J} = Ne(\underset{\sim}{v}_i - \underset{\sim}{v}_e) \tag{1.14}$$

in which case η corresponds to the resistivity as given by Spitzer (14). With this definition 1.12b becomes

$$\begin{aligned} i\omega \underset{\sim}{v}_e &= -\frac{e}{m_e}(\underset{\sim}{E} + \underset{\sim}{v}_e \times \underset{\sim}{B}_o) + \frac{e\eta}{m_e}\underset{\sim}{J} \\ &= -\frac{e}{m_e}(\underset{\sim}{E} - \eta\underset{\sim}{J} + \underset{\sim}{v}_e \times \underset{\sim}{B}_o) \end{aligned} \tag{1.15a}$$

and similarly for the ions 1.12a becomes

$$i\omega \underset{\sim}{v}_i = \frac{e}{\mu}(\underset{\sim}{E} - \eta\underset{\sim}{J} + \underset{\sim}{v}_i \times \underset{\sim}{B}_o) \quad . \tag{1.15b}$$

We now solve 1.15a for $\underset{\sim}{v}_e$ in terms of $\underset{\sim}{E} - \eta\underset{\sim}{J}$ in cylindrical coordinates, recalling that $\underset{\sim}{B}_o = B_o \underset{\sim}{e}_z$, and solve 1.15b for $\underset{\sim}{v}_i$ in terms of $\underset{\sim}{E} - \eta\underset{\sim}{J}$. The resulting expressions are substituted into

1.14 which yields a result in the form

$$\begin{pmatrix} J_r \\ J_\theta \\ J_z \end{pmatrix} = \begin{pmatrix} s_1 & is_2 & 0 \\ -is_2 & s_1 & 0 \\ 0 & 0 & s_3 \end{pmatrix} \begin{pmatrix} E_r - \eta J_r \\ E_\theta - \eta J_\theta \\ E_z - \eta J_z \end{pmatrix} \tag{1.16}$$

where

$$s_1 = \left[\frac{\omega_p^2}{\omega_c^2 - \omega^2} + \frac{\Omega_p^2}{\Omega_c^2 - \omega^2} \right] i\omega\epsilon_o \tag{1.17a}$$

$$s_2 = \left[\frac{\omega_p^2 \, \omega_c}{\omega_c^2 - \omega^2} - \frac{\Omega_p^2 \, \Omega_c}{\Omega_c^2 - \omega^2} \right] i\epsilon_o \tag{1.17b}$$

$$s_3 = \frac{\omega_p^2 + \Omega_p^2}{i\omega} \, \epsilon_o \tag{1.17c}$$

and

$$\omega_p^2 = \frac{Ne^2}{m_e \epsilon_o} , \quad \Omega_p^2 = \frac{Ne^2}{\mu\epsilon_o} , \quad \omega_c = \frac{eB_o}{m_e} , \quad \Omega_c = \frac{eB_o}{\mu} . \tag{1.18}$$

We note that when $\eta \to 0$, the above s tensor is just the conductivity tensor.

If we now solve 1.16 for $\underset{\sim}{J}$ in terms of $\underset{\sim}{E}$ alone, we obtain

$$\begin{pmatrix} J_r \\ J_\theta \\ J_z \end{pmatrix} = \begin{pmatrix} \sigma_1 & i\sigma_2 & 0 \\ -i\sigma_2 & \sigma_1 & 0 \\ 0 & 0 & \sigma_3 \end{pmatrix} \begin{pmatrix} E_r \\ E_\theta \\ E_z \end{pmatrix} \tag{1.19}$$

where

$$\sigma_1 = \frac{s_1 + \eta(s_1^2 - s_2^2)}{1 + 2\eta s_1 + \eta^2(s_1^2 - s_2^2)} \tag{1.20a}$$

$$\sigma_2 = \frac{s_2}{1 + 2\eta s_1 + \eta^2(s_1^2 - s_2^2)} \tag{1.20b}$$

$$\sigma_3 = \frac{s_3}{1 + \eta s_3} \quad . \tag{1.20c}$$

We now wish to solve Maxwell's equations where the currents are related to the fields in the above way. The pertinent Maxwell's equations are

$$\nabla \times \underset{\sim}{E} = -i\omega\mu_o \underset{\sim}{H} \tag{1.21a}$$

$$\nabla \times \underset{\sim}{H} = \underset{\sim}{J} + i\omega\epsilon_o \underset{\sim}{E} \quad . \tag{1.21b}$$

To simplify the notation we will combine the plasma current $\underset{\sim}{J} = \underset{\approx}{\sigma} \cdot \underset{\sim}{E}$ and the displacement current $i\omega\epsilon_o \underset{\sim}{E}$ into a single term by defining a dielectric tensor so that

$$i\omega \underset{\approx}{\epsilon} \cdot \underset{\sim}{E} = \underset{\approx}{\sigma} \cdot \underset{\sim}{E} + i\omega\epsilon_o \underset{\sim}{E} = i\omega \underset{\sim}{D} \quad . \tag{1.22}$$

Hence

$$\begin{pmatrix} D_r \\ D_\theta \\ D_z \end{pmatrix} = \begin{pmatrix} \epsilon_1 & i\epsilon_2 & 0 \\ -i\epsilon_2 & \epsilon_1 & 0 \\ 0 & 0 & \epsilon_3 \end{pmatrix} \begin{pmatrix} E_r \\ E_\theta \\ E_z \end{pmatrix} \tag{1.23}$$

where

$$\epsilon_1 = \epsilon_o + \frac{\sigma_1}{i\omega} \tag{1.24a}$$

$$\epsilon_2 = \frac{\sigma_2}{i\omega} \tag{1.24b}$$

$$\epsilon_3 = \epsilon_o + \frac{\sigma_3}{i\omega} \quad . \tag{1.24c}$$

All the information about the plasma is now contained in ϵ_1, ϵ_2, and ϵ_3. The problem to be solved now is Maxwell's equations in a cylindrical conducting waveguide with a dielectric tensor of the form of 1.23.

CHAPTER II

SOLUTION OF MAXWELL'S EQUATIONS IN A CYLINDRICAL WAVEGUIDE

1. Solution of the Differential Equations

Although the problem of solving Maxwell's equations with a non-diagonal dielectric tensor may be done with complete generality (15), only the circularly symmetric modes will be discussed here, since in the experiment only those modes may be excited. Using this restriction, we may now assume the fields to vary as $e^{i(\omega t - kz)}$. Writing out Maxwell's equations in component form we have

$$ikE_\theta = -i\omega\mu_o H_r \tag{2.1a}$$

$$-ikE_r - \frac{\partial E_z}{\partial r} = -i\omega\mu_o H_\theta \tag{2.1b}$$

$$\frac{1}{r}\frac{\partial}{\partial r}(rE_\theta) = -i\omega\mu_o H_z \tag{2.1c}$$

$$ikH_\theta = i\omega(\epsilon_1 E_r + i\epsilon_2 E_\theta) \tag{2.2a}$$

$$-ikH_r - \frac{\partial H_z}{\partial r} = i\omega(-i\epsilon_2 E_r + \epsilon_1 E_\theta) \tag{2.2b}$$

$$\frac{1}{r}\frac{\partial}{\partial r}(rH_\theta) = i\omega\epsilon_3 E_z \quad . \tag{2.2c}$$

It is now possible to solve this set of equations for the transverse field quantities E_r, E_θ, H_r and H_θ in terms of the longitudinal components and their spatial derivatives. For example, we might solve equation 2.1a for H_r and substitute into 2.2b, obtaining

$$i\gamma_2 E_r + \gamma_1 E_\theta = -i\omega\mu_o \frac{\partial H_z}{\partial r} \quad . \tag{2.3a}$$

Similarly we may obtain

$$\gamma_1 E_r - i\gamma_2 E_\theta = ik \frac{\partial E_z}{\partial r} \tag{2.3b}$$

$$\gamma_1 H_r - i\gamma_2 H_\theta = ik \frac{\partial H_z}{\partial r} - \omega \epsilon_2 \frac{\partial E_z}{\partial r} \tag{2.3c}$$

$$i\gamma_2 H_r + \gamma_1 H_\theta = i\omega \epsilon_1 \frac{\partial E_z}{\partial r} \tag{2.3d}$$

where $\gamma_1 \equiv k^2 - \omega^2 \mu_o \epsilon_1$ and $\gamma_2 \equiv \omega^2 \mu_o \epsilon_2$. It is clear that unless $\gamma_1^2 = \gamma_2^2$, equations 2.3a,b,c,d will allow us to solve for the transverse components in terms of the longitudinal components. The results are

$$E_r = ia \frac{\partial E_z}{\partial r} + b \frac{\partial H_z}{\partial r} \tag{2.4a}$$

$$E_\theta = c \frac{\partial E_z}{\partial r} + id \frac{\partial H_z}{\partial r} \tag{2.4b}$$

$$H_r = f \frac{\partial E_z}{\partial r} + ia \frac{\partial H_z}{\partial r} \tag{2.4c}$$

$$H_\theta = ig \frac{\partial E_z}{\partial r} + c \frac{\partial H_z}{\partial r} \tag{2.4d}$$

where

$$a \equiv \frac{k\gamma_1}{\gamma_1^2 - \gamma_2^2}, \quad b \equiv \frac{\omega\mu_o \gamma_2}{\gamma_1^2 - \gamma_2^2}, \quad c \equiv \frac{k\gamma_2}{\gamma_1^2 - \gamma_2^2}, \quad d \equiv -\frac{\omega\mu_o \gamma_1}{\gamma_1^2 - \gamma_2^2},$$

$$f \equiv \frac{\omega\epsilon_2 \gamma_1 + \omega\epsilon_1 \gamma_2}{\gamma_1^2 - \gamma_2^2}, \quad g \equiv \frac{\omega\epsilon_1 \gamma_1 + \omega\epsilon_2 \gamma_2}{\gamma_1^2 - \gamma_2^2}; \tag{2.5}$$

(note, $ab + cd = 0$, $fd - ac = 0$) .

Putting 2.4b into 2.1c and 2.4d into 2.2c we obtain the coupled pair of differential equations for E_z and H_z

$$\frac{id}{r}\frac{\partial}{\partial r}\left(\frac{r\,\partial H_z}{\partial r}\right) + i\omega\mu_o H_z + \frac{c}{r}\frac{\partial}{\partial r}\left(\frac{r\,\partial E_z}{\partial r}\right) = 0 \qquad (2.6a)$$

$$\frac{ig}{r}\frac{\partial}{\partial r}\left(\frac{r\,\partial E_z}{\partial r}\right) - i\omega\epsilon_3 E_z + \frac{c}{r}\frac{\partial}{\partial r}\left(\frac{r\,\partial H_z}{\partial r}\right) = 0 \,. \qquad (2.6b)$$

To find the solution of these coupled equations, we assume that $H_z = \phi$ and $E_z = \alpha\phi$. where α is a constant, thus obtaining

$$(id + \alpha c)\frac{1}{r}\frac{\partial}{\partial r}\left(r\frac{\partial\phi}{\partial r}\right) + i\omega\mu_o\phi = 0 \qquad (2.7a)$$

$$(ig\alpha + c)\frac{1}{r}\frac{\partial}{\partial r}\left(r\frac{\partial\phi}{\partial r}\right) - i\omega\epsilon_3\alpha\phi = 0 \,. \qquad (2.7b)$$

For these two solutions to be compatible, we must have

$$\alpha^2 + i\left(\frac{d}{c} + \frac{g}{c}\frac{\mu_o}{\epsilon_3}\right)\alpha + \frac{\mu_o}{\epsilon_3} = 0 \,. \qquad (2.8)$$

If we label the two solutions of this quadratic equation by α_1 and α_2 we have

$$H_z = \phi_1 + \phi_2 \qquad (2.9a)$$

$$E_z = \alpha_1\phi_1 + \alpha_2\phi_2 \qquad (2.9b)$$

where ϕ_1 and ϕ_2 are the solutions of the differential equations,

$$\frac{1}{r}\frac{\partial}{\partial r}\left(r\frac{\partial\phi_1}{\partial r}\right) + \left(\frac{i\omega\mu_o}{id + \alpha_1 c}\right)\phi_1 = 0 \qquad (2.10a)$$

$$\frac{1}{r}\frac{\partial}{\partial r}\left(r\frac{\partial\phi_2}{\partial r}\right) + \left(\frac{i\omega\mu_o}{id + \alpha_2 c}\right)\phi_2 = 0 \,. \qquad (2.10b)$$

For completeness we should also consider a $\phi_3 = 0$ in which case $H_z = E_z = 0$, for which we must have $\gamma_1^2 = \gamma_2^2$ for non-zero transverse fields, but we shall not consider this latter case any further since we are looking for solutions with finite H_z.

At this point we shall define a transverse wave number T so that

$$T^2 \equiv \frac{\omega \mu_o}{d - i\alpha c} \tag{2.11}$$

and solve this for α and rewrite 2.8 as a quadratic in T^2 so that

$$\frac{\omega \mu_o}{T^2 c}\left[\frac{\omega\mu_o}{T^2 c} - \frac{d}{c}\right] = \frac{\mu_o}{\epsilon_3}\left[1 - \frac{g}{c}\left(\frac{\omega\mu_o}{T^2 c} - \frac{d}{c}\right)\right] . \tag{2.12}$$

Using the definitions 2.5 for c, d and g, we obtain

$$(\gamma_1^2 - \gamma_2^2)(\gamma_1^2 - \gamma_2^2 + \gamma_1 T^2) - \frac{T^2}{\omega^2 \mu_o \epsilon_3}\left[k^2 \gamma_2^2 T^2 - (\gamma_1 k^2 - \gamma_1^2 + \gamma_2^2)(\gamma_1^2 - \gamma_2^2 + \gamma_1 T^2)\right] = 0 . \tag{2.13}$$

Upon rearranging the term in the bracket it becomes apparent that the equation has a factor $\gamma_1^2 - \gamma_2^2$, corresponding to the $\phi_3 = 0$ case mentioned above. The remaining factor gives

$$\gamma_1^2 - \gamma_2^2 + \gamma_1 T^2 - \frac{T^2}{\omega^2 \mu_o \epsilon_3}\left[\gamma_1^2 - \gamma_2^2 + \gamma_1 T^2 - k^2(\gamma_1 + T^2)\right] = 0 . \tag{2.14}$$

We note that this equation is quadratic both in γ_1 (or k^2), corresponding to two distinct modes of propagation, and in T^2 which means that there are two values of T^2 for each mode.

If we return now to construct the solutions of the differential equations, we see that both are of the form

$$\frac{1}{r}\frac{\partial}{\partial r}\left(r\frac{\partial \phi_i}{\partial r}\right) + T_i^2 \phi_i = 0 \qquad (2.15)$$

where i is either 1 or 2 . Solutions of 2.15 which are regular at the origin are,

$$\phi_1(r) = A_1 J_o(T_1 r) \qquad (2.16a)$$

$$\phi_2(r) = A_2 J_o(T_2 r) \quad . \qquad (2.16b)$$

Now for a particular mode, T_1 and T_2 are not independent since they are the two solutions of 2.14, and A_1 and A_2 are related by the boundary condition. In general, there will be a set of values of T_1 and T_2 which separately satisfy 2.14 and the boundary condition, and a superposition of those solutions so constructed is also a solution, so that the general solution may be written

$$H_z(r) = \sum_m A_m \left[J_o(T_{1m} r) + \tau_m J_o(T_{2m} r) \right] \qquad (2.17a)$$

$$E_z(r) = \sum_m A_m \left[\alpha_{1m} J_o(T_{1m} r) + \tau_m \alpha_{2m} J_o(T_{2m} r) \right] \qquad (2.17b)$$

where the T_{1m}, T_{2m} and τ_m are determined by the boundary condition along with 2.14 and the A_m are amplitude coefficients determined by the particular type of excitation.

From the expressions 2.17a,b, using the relations 2.4a,b,c,d, we can now construct all the field components. The results after simplification are

$$H_z(r,z,t) = \sum_m A_m \left[J_o(T_{1m}r) + \tau_m J_o(T_{2m}r) \right] e^{i(\omega t - k_m z)} \tag{2.18a}$$

$$H_r(r,z,t) = \sum_m A_m ik_m \left[\frac{J_1(T_{1m}r)}{T_{1m}} + \tau_m \frac{J_1(T_{2m}r)}{T_{2m}} \right] e^{i(\omega t - k_m z)} \tag{2.18b}$$

$$H_\theta(r,z,t) = \sum_m \frac{A_m \epsilon_1}{k_m \epsilon_2} \left[\beta_{1m} \frac{J_1(T_{1m}r)}{T_{1m}} + \tau_m \beta_{2m} \frac{J_1(T_{2m}r)}{T_{2m}} \right] e^{i(\omega t - k_m z)} \tag{2.18c}$$

$$E_z(r,z,t) = \sum_m \frac{A_m \epsilon_1}{i\omega k_m \epsilon_2 \epsilon_3} \left[\beta_{1m} J_o(T_{1m}r) + \tau_m \beta_{2m} J_o(T_{2m}r) \right] e^{i(\omega t - k_m z)} \tag{2.19a}$$

$$E_r(r,z,t) = \sum_m \frac{A_m}{\omega \epsilon_2} \left[(\gamma_{1m} + T_{1m}^2) \frac{J_1(T_{1m}r)}{T_{1m}} + \tau_m (\gamma_{1m} + T_{2m}^2) \frac{J_1(T_{2m}r)}{T_{2m}} \right] \times e^{i(\omega t - k_m z)} \tag{2.19b}$$

$$E_\theta(r,z,t) = \sum_m - A_m i\omega\mu_o \left[\frac{J_1(T_{1m}r)}{T_{1m}} + \tau_m \frac{J_1(T_{2m}r)}{T_{2m}} \right] e^{i(\omega t - k_m z)} \tag{2.19c}$$

where in general the A_m are functions of ω, and

$$\beta_{1m} \equiv \gamma_{1m} + \frac{\gamma_2 \epsilon_2}{\epsilon_1} + T_{1m}^2 \tag{2.20a}$$

$$\beta_{2m} \equiv \gamma_{1m} + \frac{\gamma_2 \epsilon_2}{\epsilon_1} + T_{2m}^2 \quad . \tag{2.20b}$$

2. Solution of the Boundary Value Problem

In the solution of the boundary value problem we shall treat one mode at a time since each must satisfy the boundary condition separately. We shall drop the m subscript in the following analysis, although the results will be true for any of the m circularly symmetric modes.

For our boundary condition we assume that our waveguide is a cylindrical conducting tube of radius a so that we have for the tangential E fields

$$E_\theta(a) = E_z(a) = 0 \quad . \tag{2.21}$$

Using the expressions 2.19a,c we obtain

$$\frac{J_1(T_1 a)}{T_1} + \tau \frac{J_1(T_2 a)}{T_2} = 0 \tag{2.22a}$$

$$\beta_1 J_o(T_1 a) + \tau\beta_2 J_o(T_2 a) = 0 \quad . \tag{2.22b}$$

We may use 2.22a to determine τ so that

$$\tau = - \frac{T_2 J_1(T_1 a)}{T_1 J_1(T_2 a)} \tag{2.23}$$

and we then obtain from 2.22b

$$\beta_1 T_1 J_o(T_1 a)\, J_1(T_2 a) = \beta_2 T_2 J_o(T_2 a)\, J_1(T_1 a) \quad . \tag{2.24}$$

This equation is now to be solved simultaneously with 2.14 to obtain the dispersion relation. We may rearrange 2.14 and present it in the form

$$\gamma_1^2 - \gamma_2^2 + \gamma_1 T^2 + \frac{\epsilon_1 T^2}{\epsilon_3} \left(\gamma_1 + \frac{\gamma_2 \epsilon_2}{\epsilon_1} + T^2\right) = 0 \tag{2.25}$$

but the set 2.24 and 2.25 is transcendental and, except in certain limiting cases, an approximate solution is very difficult to obtain without a computer.

3. Solution of the Dispersion Relation at Low Frequencies

If we neglect dissipation it may be shown that for frequencies of the order of Ω_c, ϵ_1 and ϵ_2 are of the order of $\epsilon_o \frac{c^2}{V_A^2}$ and $-\epsilon_o \frac{c^2}{V_A^2}\frac{\omega}{\Omega_c}$ respectively, where

$$V_A = B_o/\sqrt{\mu_o N_i m_i} \quad , \tag{2.26}$$

the ordinary Alfven speed. But ϵ_3 is of the order $-\epsilon_o \frac{\omega_p^2}{\omega^2}$ so that ϵ_1/ϵ_3 is of the order of $-c^2\omega^2/\omega_p^2 V_A^2 = -(\omega^2/\Omega_c^2)\frac{m_e}{m_i}$, which we will take to be of the order of m_e/m_i. If we then neglect terms of the order m_e/m_i in 2.25, we get

$$\gamma_1^2 - \gamma_2^2 + \gamma_1 T^2 = 0 \quad . \tag{2.27}$$

Using 2.27 we find from 2.11 that $\alpha = 0$, so $E_z = 0$, and we have simply that

$$\phi(r) = \sum_m A_m J_o(T_m r) \quad . \tag{2.28}$$

The boundary condition for each mode now becomes

$$E_{\theta m}(a) = -A_m \frac{i\omega\mu_o}{T_m} J_1(T_m a) = 0 \quad , \tag{2.29}$$

so that the T_m are derived from the roots of the first order Bessel function (i.e., Ta = 3.83, 7.01, 10.17, etc.). With T^2 known, we may now solve 2.27 for k^2 and we obtain

$$k^2 = \omega^2\mu_o\epsilon_1 - \frac{T^2}{2} + \sqrt{\left(\frac{T^2}{2}\right)^2 + (\omega^2\mu_o\epsilon_2)^2} \qquad (2.30a)$$

$$k^2 = \omega^2\mu_o\epsilon_1 - \frac{T^2}{2} - \sqrt{\left(\frac{T^2}{2}\right)^2 + (\omega^2\mu_o\epsilon_o)^2} \quad . \qquad (2.30b)$$

It is to be noted that the value of T_m is the same for both roots of 2.27, so that both modes are characterized by the roots of the first order Bessel function.

If we now, however, investigate the limit when $\omega \ll \Omega_c$, then another approximation is pertinent, namely that $\epsilon_2 \ll \epsilon_1$ since $\epsilon_2^2/\epsilon_1^2$ is of the order of ω^2/Ω_c^2. This is especially appropriate when dissipation is present, since if we assume an electron-ion collision frequency $\nu_{ei} \gg \omega$, then ϵ_1/ϵ_3 is of the order of $-i(\frac{\omega}{\Omega_c})(\frac{\nu_{ei}}{\omega_c})$. Hence if ν_{ei}/ω_c is of the order of unity, then ϵ_1/ϵ_3 only goes to zero as ω/Ω_c, whereas $\epsilon_2^2/\epsilon_1^2$ goes as $(\omega/\Omega_c)^2$. If we then drop γ_2 and ϵ_2 from 2.25, the result may be factored as

$$(\gamma_1 + \frac{\epsilon_1}{\epsilon_3} T^2)(\gamma_1 + T^2) = 0 \qquad (2.31)$$

where the first factor corresponds to the root 2.30a and the second factor to the root 2.30b. The fact that the result 2.31 appears in factored form, however, implies that the original differential equations are uncoupled, and indeed, upon going back to the expressions 2.1abc and 2.2abc we find that, setting $\epsilon_2 = 0$,

$$H_\theta = \frac{i\omega\epsilon_1}{\gamma_1} \frac{\partial E_z}{\partial r} \qquad (2.32a)$$

$$E_r = \frac{ik}{\gamma_1} \frac{\partial E_z}{\partial r} \tag{2.32b}$$

$$\frac{1}{r} \frac{\partial}{\partial r} \left(r \frac{\partial E_z}{\partial r} \right) - \frac{\gamma_1 \epsilon_3}{\epsilon_1} E_z = 0 \tag{2.32c}$$

and

$$H_r = \frac{ik}{\gamma_1} \frac{\partial H_z}{\partial r} \tag{2.33a}$$

$$E_\theta = - \frac{i\omega\mu_o}{\gamma_1} \frac{\partial H_z}{\partial r} \tag{2.33b}$$

$$\frac{1}{r} \frac{\partial}{\partial r} \left(r \frac{\partial H_z}{\partial r} \right) - \gamma_1 H_z = 0 \quad . \tag{2.33c}$$

If now we let

$$T_1^2 = - \frac{\gamma_1 \epsilon_3}{\epsilon_1} \tag{2.34}$$

we have

$$E_z(r) = \sum_m A_m J_o(T_{1m} r) \tag{2.35}$$

and the boundary condition is

$$E_{zm}(a) = A_m J_o(T_{1m} r) = 0 \tag{2.36}$$

whereas, if we let

$$T_2^2 = - \gamma_1 \tag{2.37}$$

we have

$$H_z(r) = \sum_m B_m J_o(T_{2m} r) \tag{2.38}$$

and for the boundary condition we have

$$E_{\theta m}(a) = - \frac{i\omega\mu_o T_{2m}}{\gamma_1} J_1(T_{2m}a) = 0 \quad . \tag{2.39}$$

We now notice that 2.39 is the same result as 2.29, so that this mode maintains the same value of T from low frequencies up to the order of the ion-cyclotron frequency (and, in fact, even to much higher frequencies). The other mode, however, has its characteristic Ta change from a root of the zero-order Bessel function to a root of the first order Bessel function.

If we examine the fields associated with the two modes we first notice that for the mode described by 2.32abc, the steady field is perturbed only in the theta direction, so the wave may be described as a Torsional Wave, and its dispersion relation is that of the ordinary Alfvén wave at low frequencies. This mode has been studied experimentally by Jephcott (9), Wilcox (10), and theoretically by many.

The other mode has a component of the wave magnetic field in the direction of the steady field, so that the field lines are alternately compressed and expanded; consequently we may describe it as a Compressional Wave, and its dispersion relation at low frequencies is given by

$$k^2 = \frac{\omega^2}{V_A^2} - T^2 \quad . \tag{2.40}$$

It is apparent from the above expression that below a critical frequency

$$\omega_o = TV_A \quad , \tag{2.41}$$

no waves propagate, (i.e., they are evanescent). This character is entirely analogous to the ordinary waveguide cutoff phenomena except that we have an effective dielectric constant $\kappa = c^2/V_A^2$.

4. Solution of the Dispersion Relation on the IBM 7090 Computer

In the solution of the exact dispersion relation (i.e., exact within the approximations of Chapter I), an iterative technique was developed which was based on the assumption that T varies slowly with frequency. The solution is started at a low frequency where the trial value of T is given by either 2.36 for the torsional waves or by 2.39 for the compressional waves. The corrected value of T after going through the iteration procedure is then used as the trial value at the next higher frequency, and the process proceeds stepwise in frequency to as high a frequency as desired.

The basic expansion in the iteration procedure is

$$\gamma_1 = \gamma_{10}(1 + \delta) \qquad \delta \ll 1 \quad . \tag{2.42}$$

The value of γ_{10} (and from it all other zero order quantities) is given by using T_{10} , the trial T , in 2.25 and solving for the root which corresponds to the mode of interest.

If we now solve 2.25 for T_1 and T_2 in terms of γ_1 , we get, keeping terms of first order in δ ,

$$T_1 = T_{10}(1 - \kappa_1\delta) \tag{2.43a}$$

$$T_2 = T_{20}(1 - \kappa_2\delta) \tag{2.43b}$$

where T_{20} is the alternate root of 2.25 and is given by

$$T_{20}^2 = -\left[T_{10}^2 + \gamma_{10}\left(1 + \frac{\epsilon_3}{\epsilon_1}\right) + \frac{\epsilon_2 \gamma_2}{\epsilon_1} \right] \tag{2.44}$$

and

$$\kappa_1 = \frac{\gamma_{10}^2 + \frac{\gamma_{10} T_{10}^2}{2}\left(1 + \frac{\epsilon_1}{\epsilon_3}\right)}{\gamma_2^2 - \gamma_{10}^2 + \frac{\epsilon_1}{\epsilon_3} T_{10}^4} \tag{2.45a}$$

$$\kappa_2 = \frac{\gamma_{10}^2 + \frac{\gamma_{10} T_{20}^2}{2}\left(1 + \frac{\epsilon_1}{\epsilon_3}\right)}{\gamma_2^2 - \gamma_{10}^2 + \frac{\epsilon_1}{\epsilon_3} T_{20}^4} \quad . \tag{2.45b}$$

Using 2.20a and 2.20b with 2.42, 2.43a,b, we have

$$\beta_1 = \beta_{10} + (\gamma_{10} - 2\kappa_1 T_{10}^2)\delta \tag{2.46a}$$

$$\beta_2 = \beta_{20} + (\gamma_{10} - 2\kappa_2 T_{20}^2)\delta \quad . \tag{2.46b}$$

If we now use all these expressions in 2.24 and expand the Bessel functions in a series about $T_{10}a$ and $T_{20}a$, keeping only first order terms in δ, we may finally solve for δ, obtaining

$$\delta = \frac{\beta_{10} T_{10} J_o(T_{10}a) J_1(T_{20}a) - \beta_{20} T_{20} J_o(T_{20}a) J_1(T_{10}a)}{A J_o(T_{10}a) J_1(T_{20}a) + B J_o(T_{20}a) J_1(T_{10}a) + C J_o(T_{10}a) J_o(T_{20}a) + D J_1(T_{10}a) J_1(T_{20}a)} \tag{2.47}$$

where

$$A = T_{10}\left[(\kappa_1 - \kappa_2)\beta_{10} + 2\kappa_1 T_{10}^2 - \gamma_{10}\right] \tag{2.48a}$$

$$B = T_{20}\left[(\kappa_1 - \kappa_2)\beta_{20} - 2\kappa_2 T_{20}^2 + \gamma_{10}\right] \tag{2.48b}$$

$$C = T_{10}T_{20}a(\kappa_2\beta_{10} - \kappa_1\beta_{20}) \tag{2.48c}$$

$$D = \kappa_2\beta_{20}T_{20}^2 a - \kappa_1\beta_{10}T_{10}^2 a \quad . \tag{2.48d}$$

Now although the formal expansion was about γ_{10}, which was chosen for symmetry reasons, the value of δ is used to improve the trial value of T_{10} by 2.43. The T_1 so computed is used as T_{10} and the process is repeated until δ is as small as desired. Examples of k, T_{11} and T_{21} for the compressional and torsional modes are given in Figures 1abc and 2abc.

5. The Impulse Response of the System

We now consider the impulse response of the system for excitation by a current loop at the plane $z = 0$ with radius b in a waveguide of radius a (see Figure 3). In order to compute the excitation coefficient for any of the m modes, we need to know the orthogonality relations, and these are quite complex for this problem. Nevertheless, they have been worked out by A. G. Lieberman, and using them he has obtained (15)

$$A_m = \frac{-I_o b\ \tilde{\mathcal{E}}_{\theta m}(b)}{\int_0^a (\underset{\sim}{\mathcal{E}}_m \times \underset{\sim}{\tilde{\mathcal{H}}}_m + \underset{\sim}{\tilde{\mathcal{E}}}_m \times \underset{\sim}{\mathcal{H}}_m) \cdot \underset{\sim}{\mathbf{e}}_z \, r\,dr} \tag{2.49}$$

where the script notation implies the expressions of 2.18abc and 2.19abc

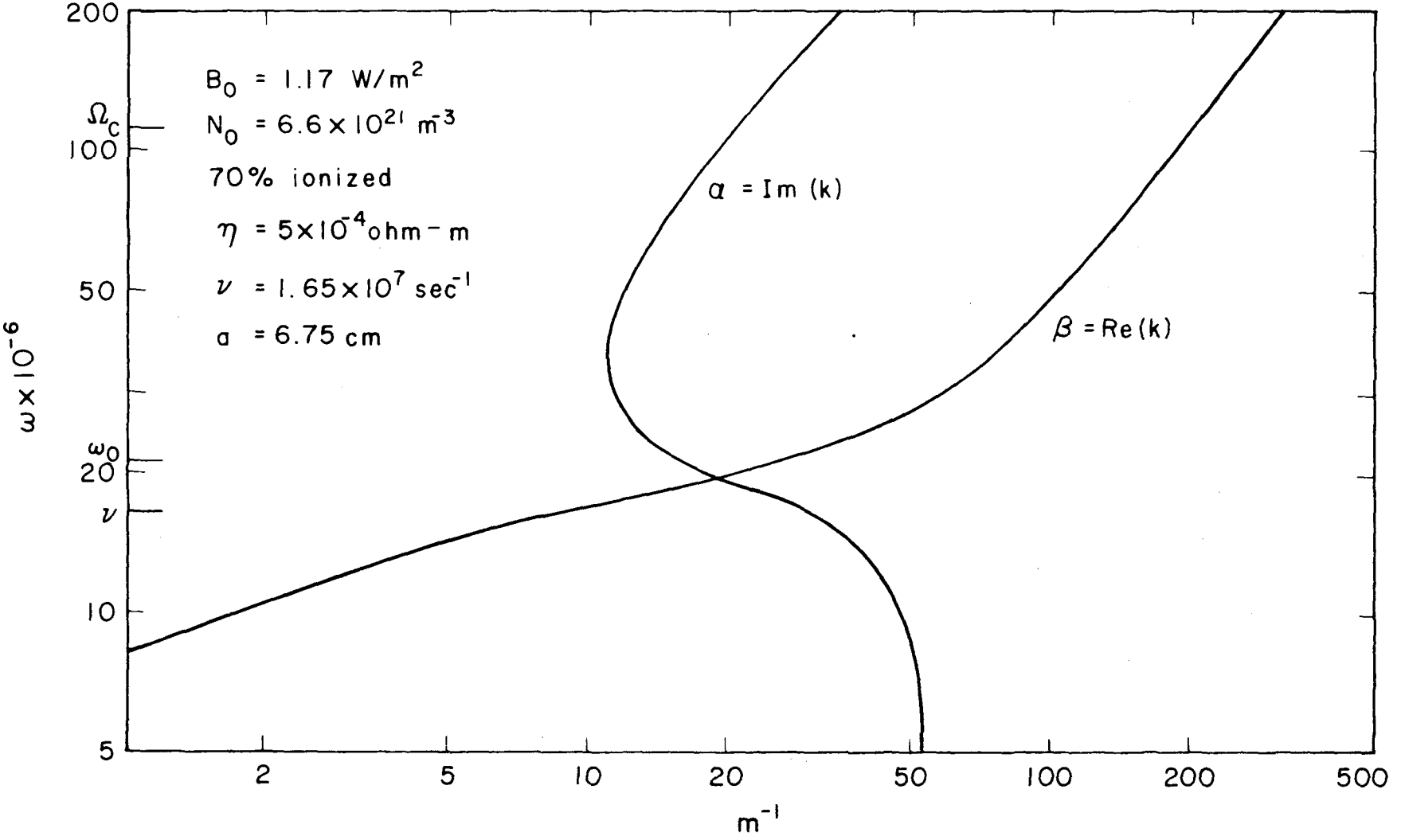

Figure 13. Frequency vs. $k = \beta - i\alpha$ for compressional mode

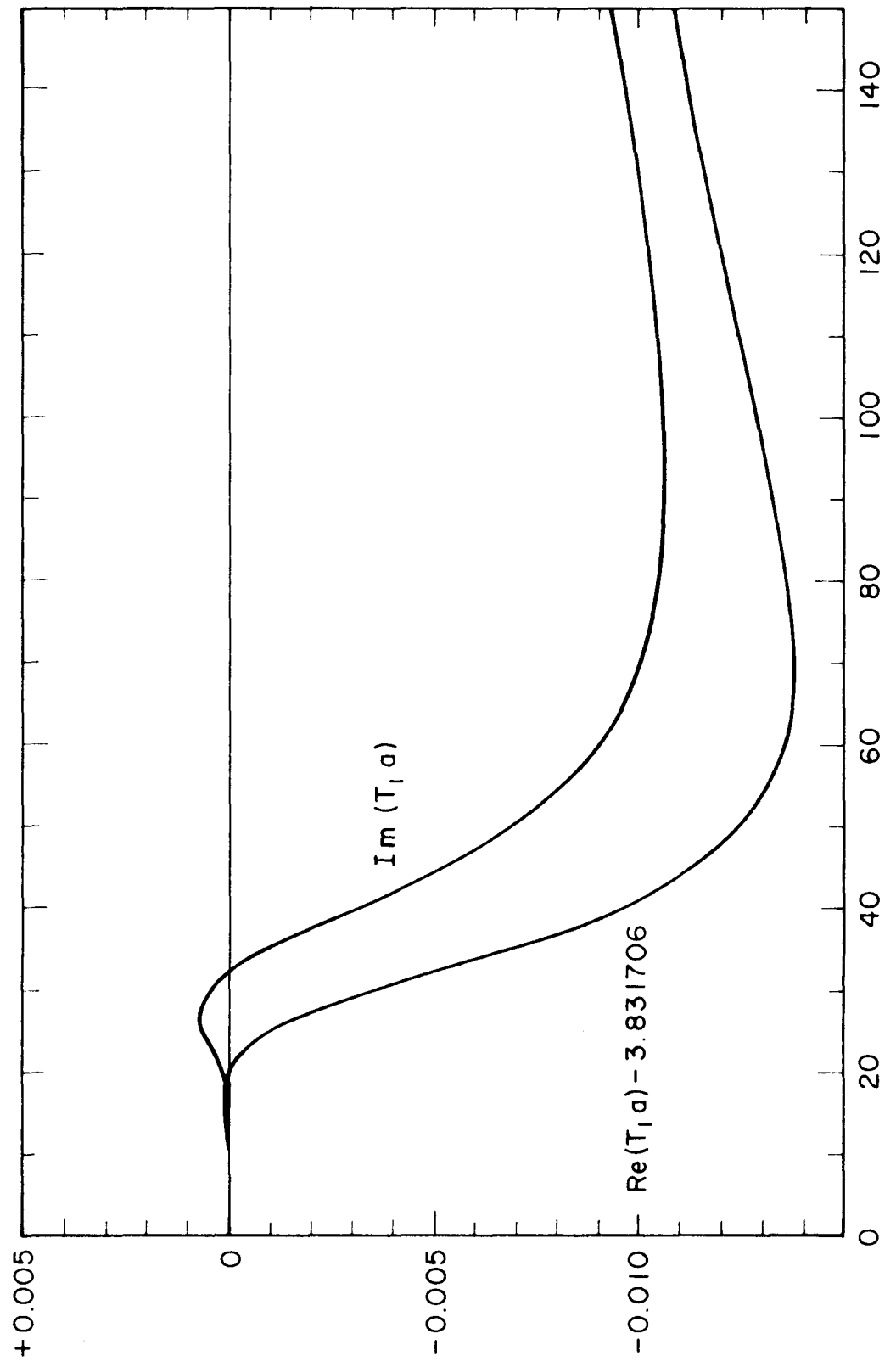

Figure 1b. $T_1 a$ vs. ω for Compressional Mode

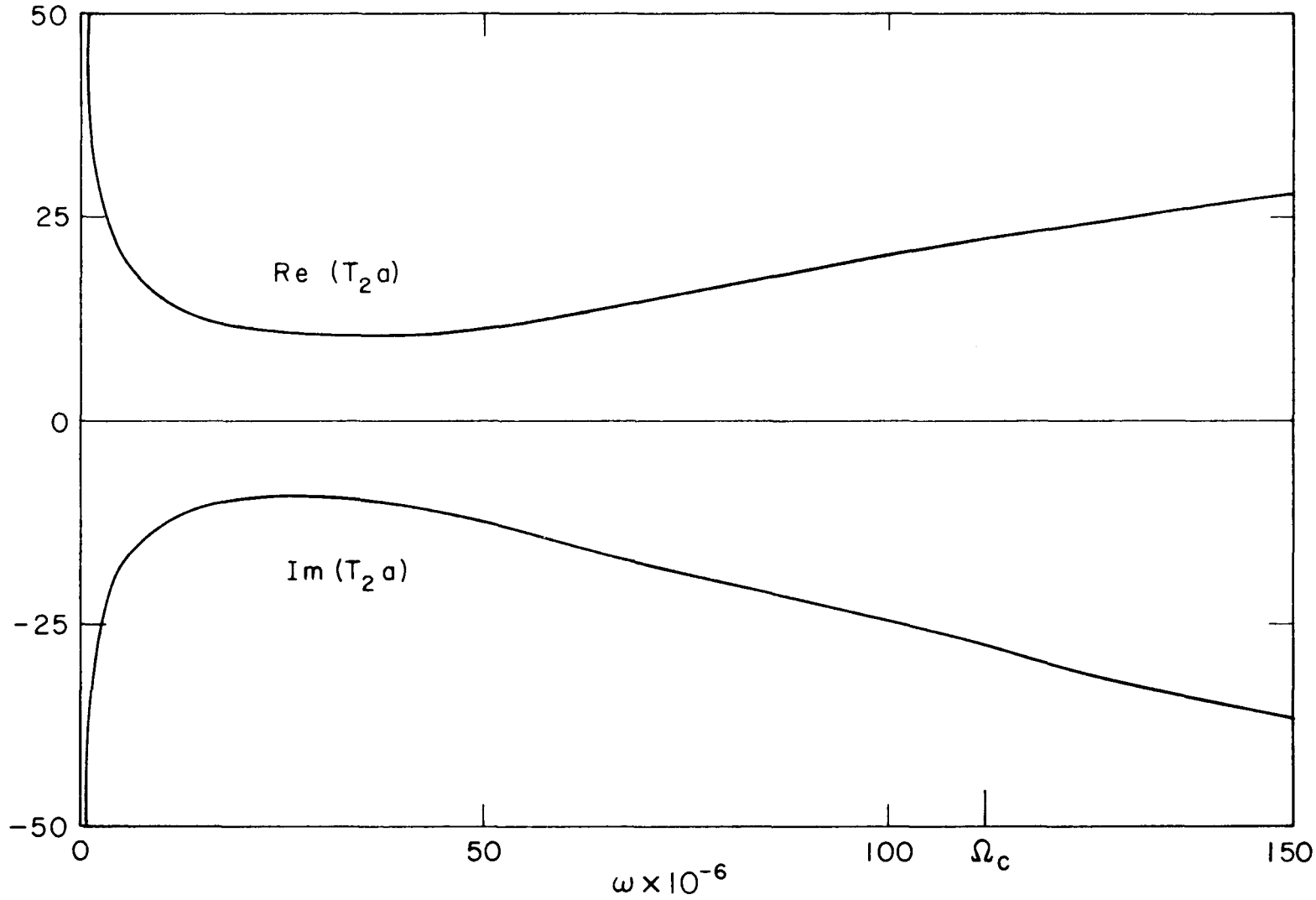

Figure 1c. T_2a vs. ω for compressional mode

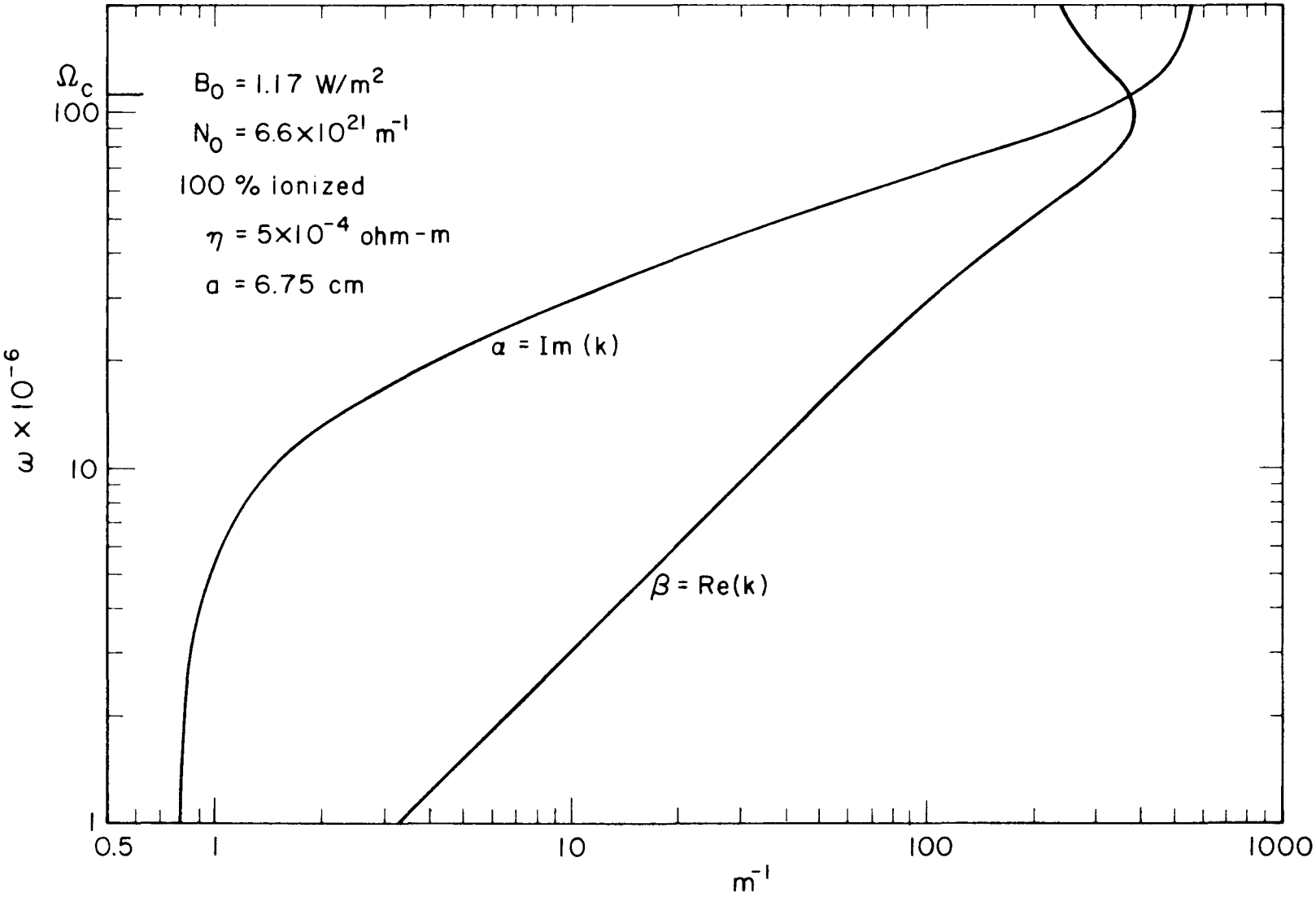

Figure 2a. **Frequency vs. propagation constant $k = \beta - i\alpha$ for the torsional mode**

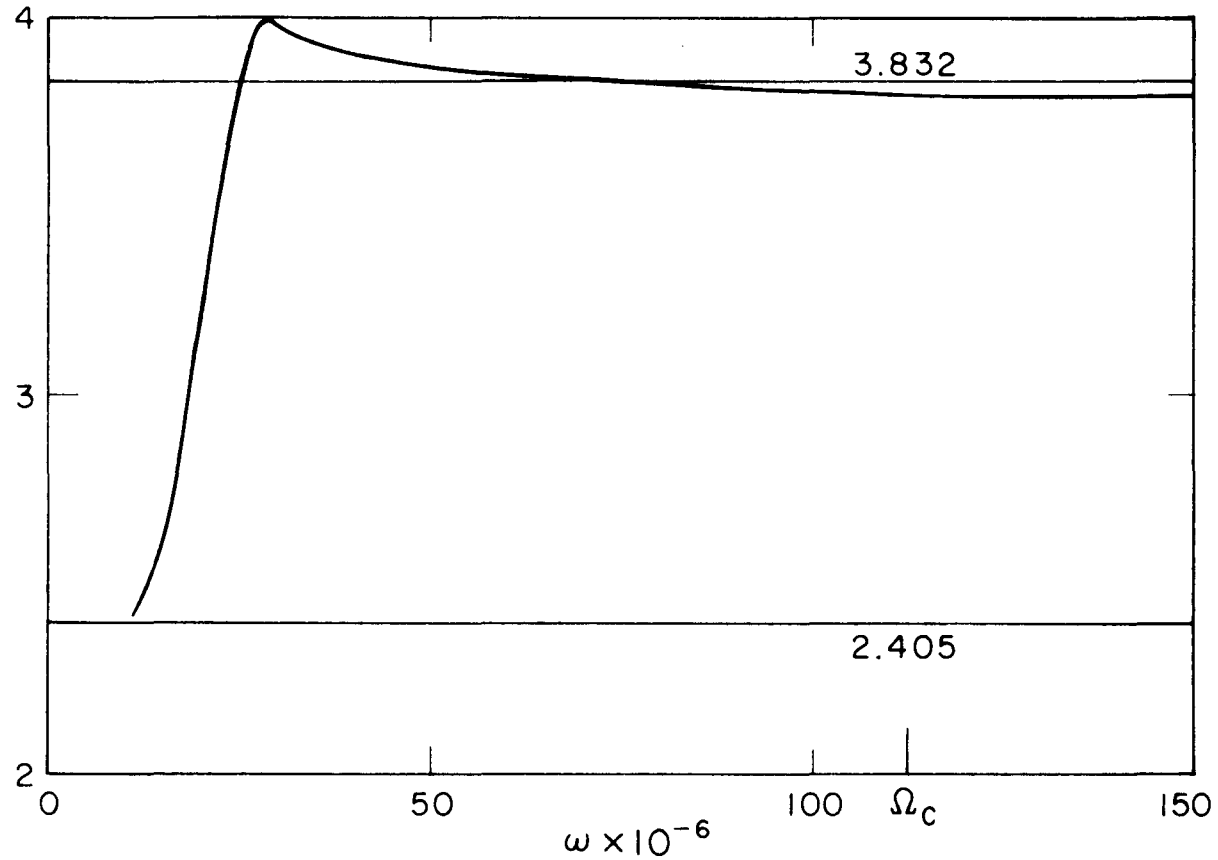

$Re(T_1 a)$ vs. ω for Torsional Mode

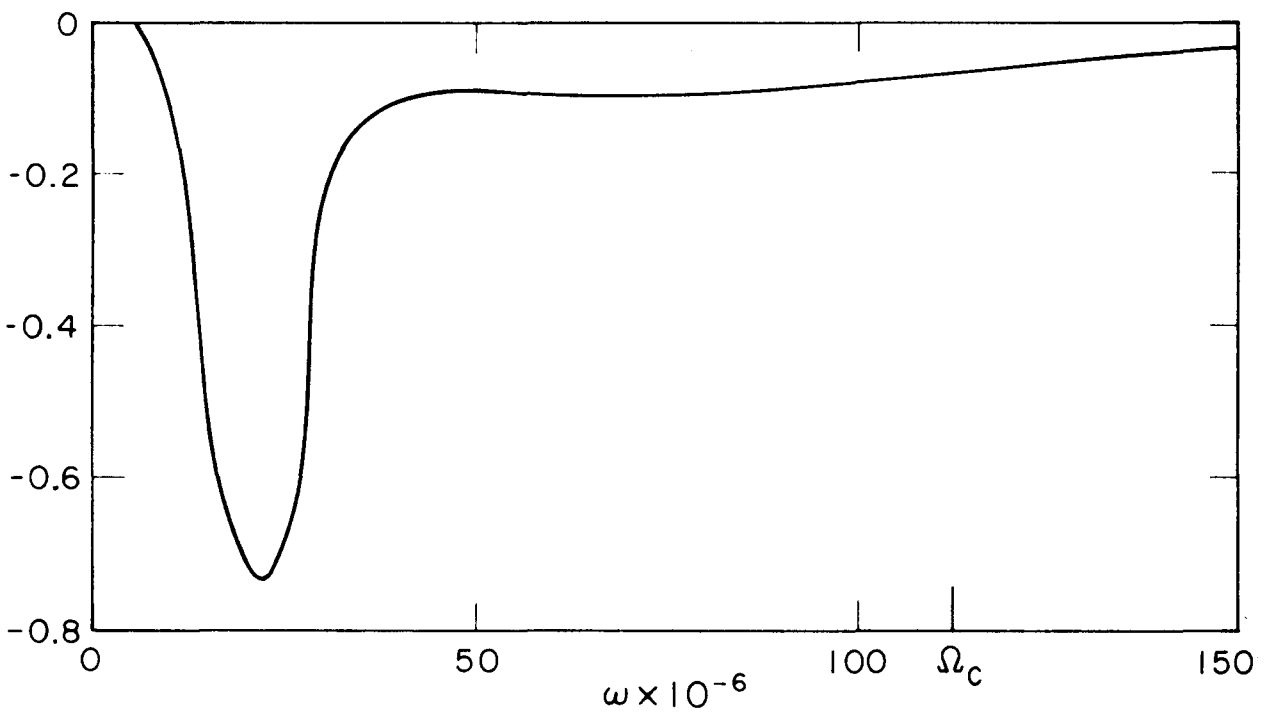

$Im(T_1 a)$ vs. ω for Torsional Mode

Figure 2b.

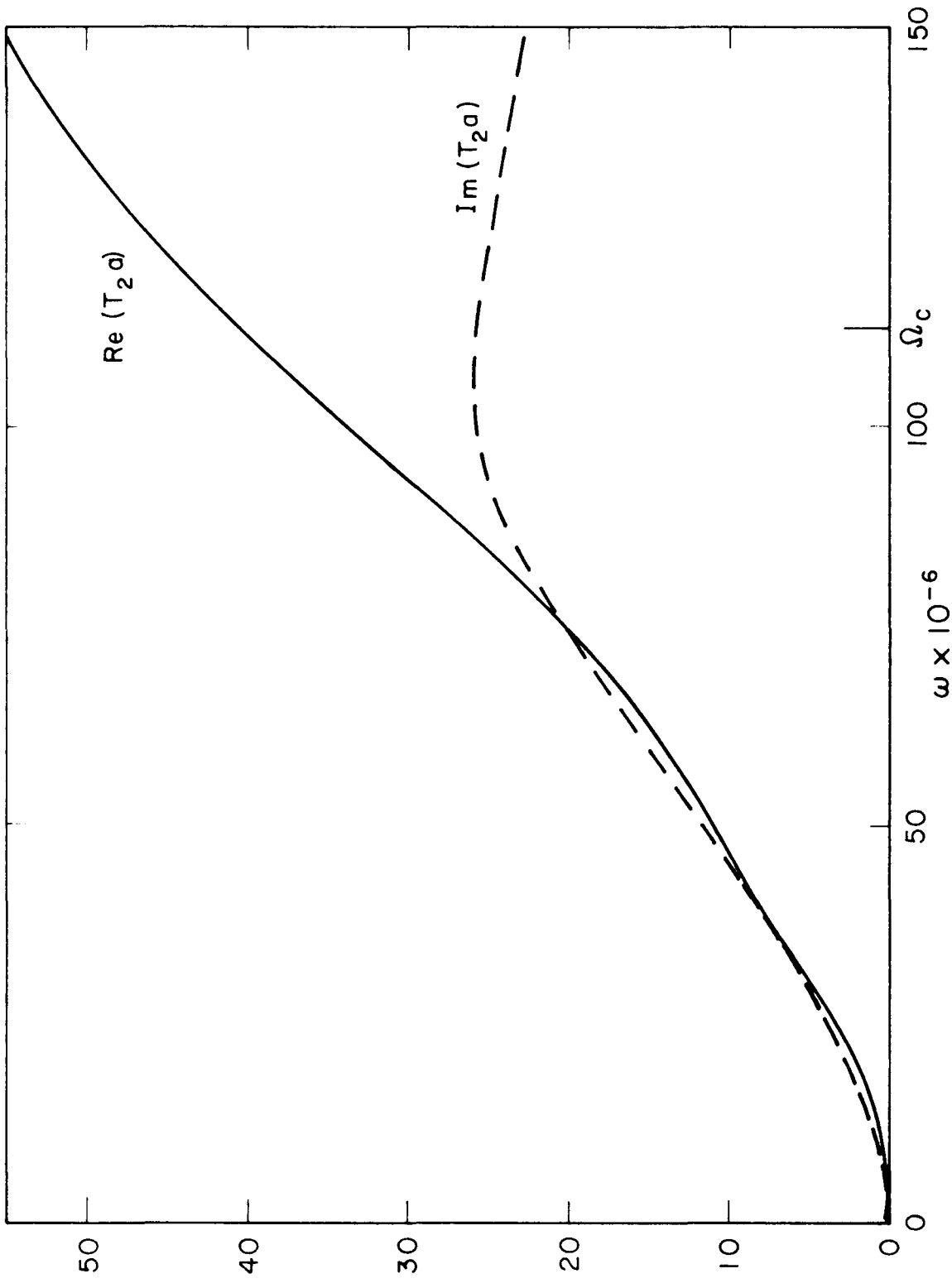

Figure 2c. T_{2a} vs. ω for Torsional Mode

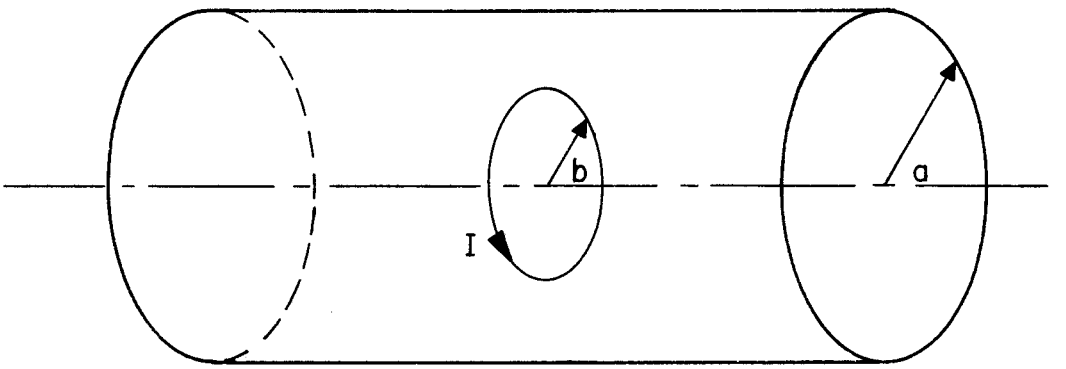

Figure 3. Current carrying loop of radius b in conducting cylinder of radius a .

without the A_m , and the tilde implies a transpose in the sense of considering B_o to point in the opposite direction, so that

$$\tilde{f}(B_o) = f(-B_o) \quad . \tag{2.50}$$

This corresponds to setting ω_c and Ω_c to $-\omega_c$ and $-\Omega_c$ respectively, and we find that the result is to change ϵ_2 to $-\epsilon_2$, and all other quantities are even in B_o . Hence

$$\tilde{\mathcal{E}}_r = -\mathcal{E}_r \tag{2.51a}$$

$$\tilde{\mathcal{E}}_\theta = \mathcal{E}_\theta \tag{2.51b}$$

$$\tilde{\mathcal{H}}_r = \mathcal{H}_r \tag{2.51c}$$

$$\tilde{\mathcal{H}}_\theta = -\mathcal{H}_\theta \tag{2.51d}$$

so that 2.49 becomes

$$A_m = \frac{-\, I_o\, b\, \mathcal{E}_{\theta m}(b)}{2\int_0^a (\mathcal{E}_{rm}\mathcal{H}_{\theta m} + \mathcal{E}_{\theta m}\mathcal{H}_{rm})\, r\, dr} \quad . \tag{2.52}$$

This expression assumes $I = I_o e^{i\omega t}$. To find the impulse response of the system, we first note that the steady state response for H_z, for example, is given by

$$H_z(r,z,t) = A_m \left[J_o(T_{1m} r) + \tau_m J_o(T_{2m} r) \right] e^{i(\omega t - kz)} \tag{2.53}$$

so that the impulse response is given by

$$H_{zm}(r,z,t) = \int_{-\infty}^{\infty} A_m(\omega) \left[J_o(T_{1m} r) + \tau_m J_o(T_{2m} r) \right] e^{i(\omega t - kz)} \frac{d\omega}{2\pi} \tag{2.54}$$

and if we wish to study the response to something other than an impulse of current, we simply use $I(\omega)$ instead of I_o in equation 2.52; and if we want the time-derivative of the magnetic field which would be detected by a magnetic probe we simply use $i\omega\, I(\omega)$ instead of I_o in 2.52 and 2.54. An example of a typical response to a critically damped sine wave for the compressional mode is shown in Figure 4.

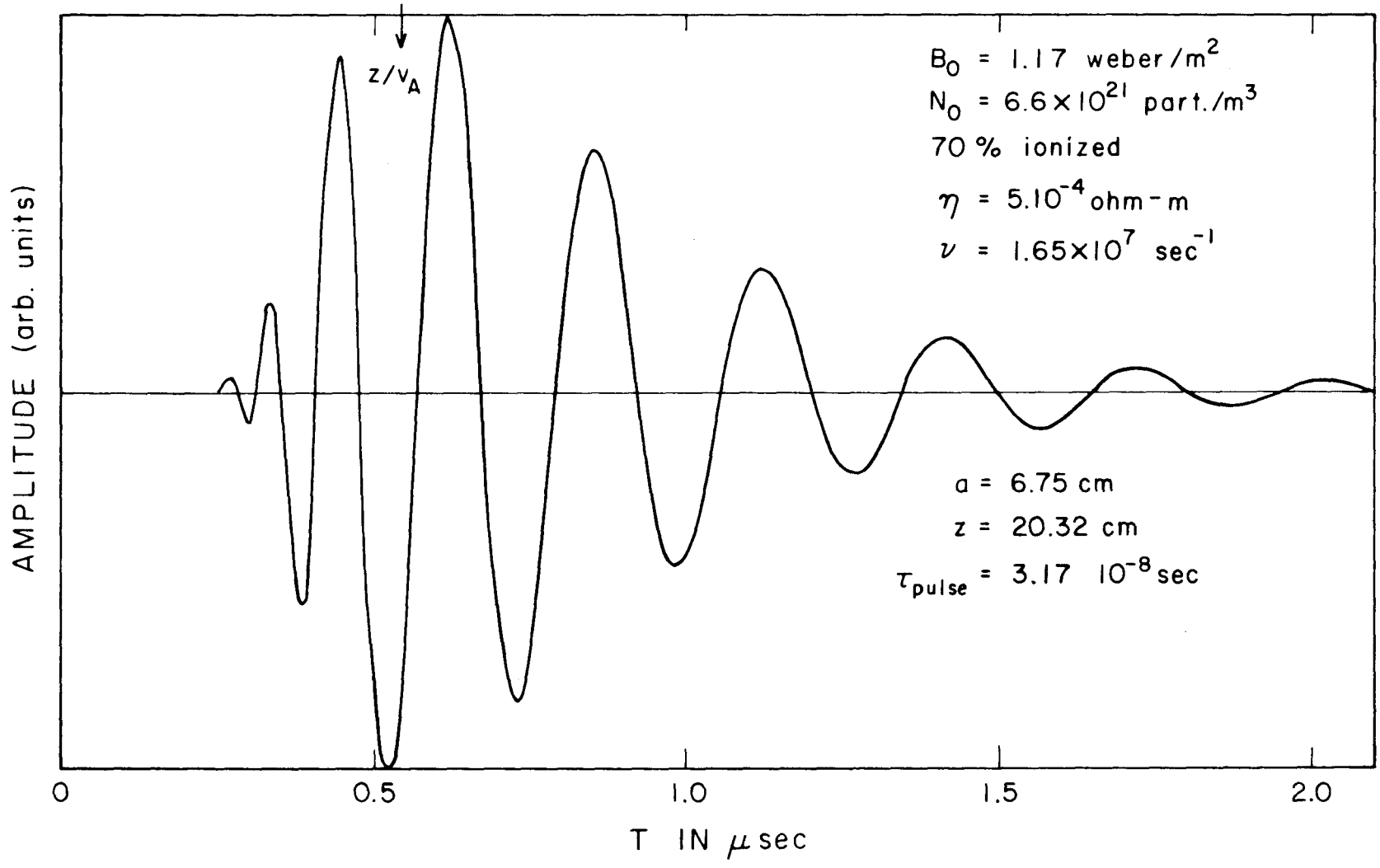

Figure 4, Response to Critically Damped Sine Wave

CHAPTER III

EXPERIMENTAL METHOD

In attempting to realize experimentally an axially magnetized plasma-filled waveguide, we have chosen a cylindrical tube because of the difficulties involved in forming a plasma in other geometries, and since a uniform cylindrical field can be produced easily with a solenoid. Waves may then be launched in the waveguide with a current loop at a specified radius and observed with small magnetic probes elsewhere in the waveguide.

1. Apparatus

The hydromagnetic waveguide is a stainless steel tube (Figure 5) 13.5 cm ID and 91.5 cm long with a 2.5 mm wall. The driving end is closed with a 1-inch thick pyrex plate through which is placed a coaxial stainless steel electrode. The opposite end connects to a section of 6-inch glass pipe which is blanked off at the end with a 1/2-inch pyrex plate and has a 2-inch side port to the vacuum pump.

The magnetic field is supplied by a pulsed double layered solenoid fabricated with 3/16-inch square copper wire and epoxy-fiberglass laminate. The energy is stored in a 1200 μfd, 10 kv bank and switched by two parallel ignitions. To prevent voltage reversal, two parallel crowbar ignitrons are also used. The basic frequency is about 350 cycles per second so that the field is within 1% of its maximum value for about 90 μseconds. The stainless steel tube and the hollow stainless steel electrode were chosen because of the high resistivity of stainless steel so that the magnetic field could penetrate the waveguide. The field

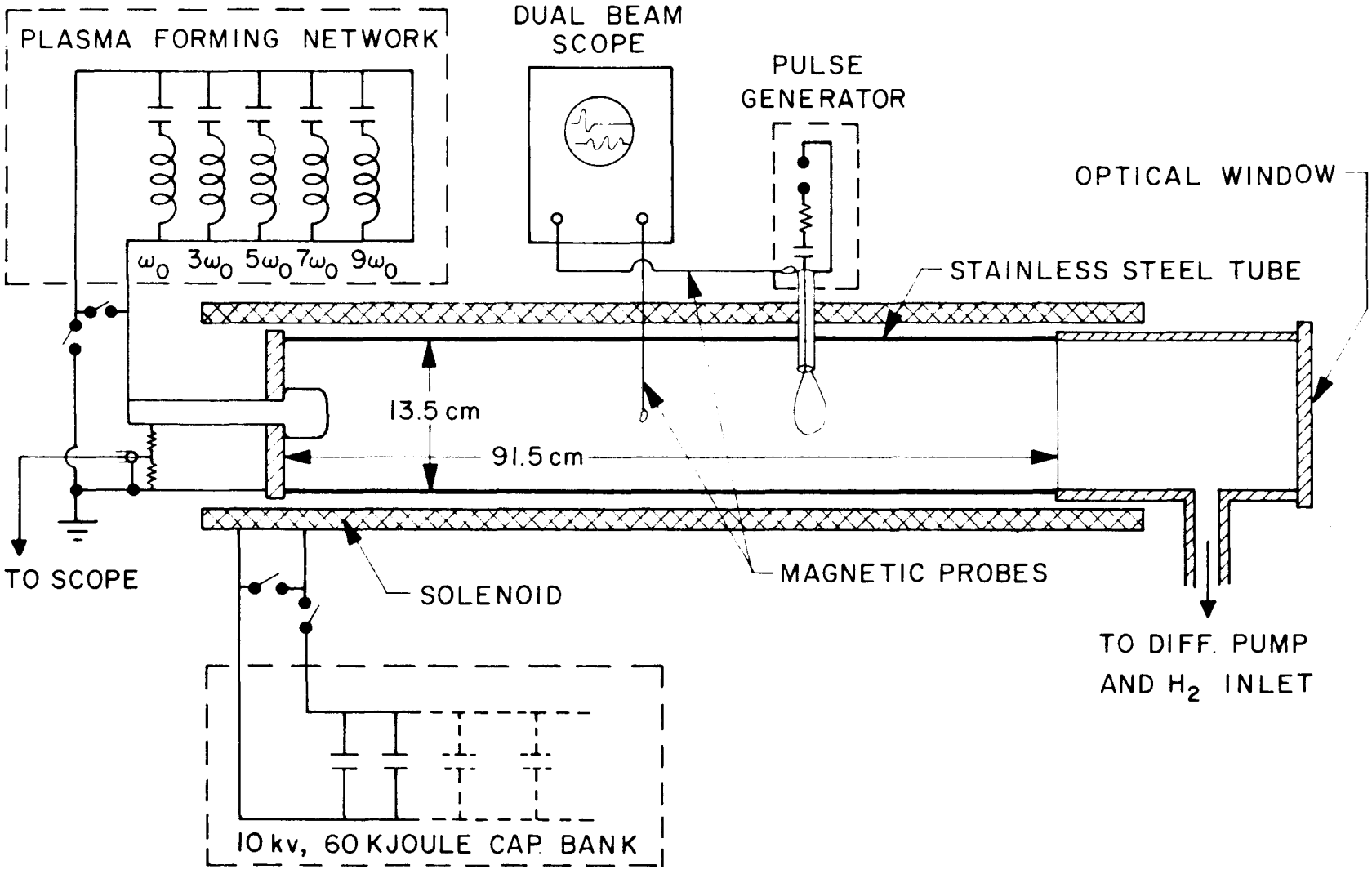

Figure 5. Schematic of Experimental Apparatus

inside the tube does reach above 90% of the value it would attain if the tube were absent. To improve the homogeneity of the field, several extra compensating turns appear at each end of the solenoid. The homogeneity has been measured to lie within 2% of the center value over more than 80 cm of the tube. The field has been calibrated to within 2%.

The vacuum pumping system consists of a 2-inch oil diffusion pump backed with a 5 cfm mechanical pump, a water-cooled baffle and a 2-inch liquid nitrogen trap. The ultimate pressure is approximately $2 \cdot 10^{-6}$ Torr. For the experiment the pump is valved off and hydrogen is leaked in to the desired pressure as measured with a Pirani gauge which was calibrated against a McLeod gauge. Between runs the system is evaculated below $5 \cdot 10^{-5}$ Torr.

The ionization energy is supplied by a 35 μsec square wave pulse network, synthesized by Fourier harmonics, so that the fundamental LC circuit has a period of 70 μsec, or $f_o = 14.3$ kilocycles, and the next has a frequency $f_1 = 3f_o$, etc., up to the fifth odd harmonic where each successive capacitor stores less energy. The inductors are tuned for a flat top on the square pulse. The characteristic impedance of the network is approximately .75 ohms, but the plasma appears to be approximately .05 ohms, so the pulse network acts as a current generator, once the voltage causes a breakdown between the electrode and the wall. At 12 kv the network stores about $1.25 \cdot 10^3$ joules, and runs about 14k amp into the plasma when switched on by an ignitron.. To control the duration of the current pulse, a crowbar is placed across the output and can be controlled to 1 μsec or less. A resistive

voltage divider allows the electrode voltage to be monitored, and a current transformer is used to monitor the current.

2. Plasma Formation

When the pulse network is switched on with an ignitron, the full charging voltage appears between the coaxial electrode and the wall of the waveguide. A local breakdown occurs quickly (within 1 μsec except at low pressures) at the driving end, and then an ionizing wave forms and travels down the tube. This wave has a well-defined front and travels very nearly at constant velocity (typically, 5 cm/μsec) if there are no serious obstructions in the tube. This type of shock wave has been studied theoretically by Kunkel and Gross (16) for a slab geometry and the theory says the velocity should be constant if the current is constant. The shock front is very narrow (approx. 1-2 cm) and behind the front the plasma is left rotating due to the $\underset{\sim}{J} \times \underset{\sim}{B}_o$ forces. For the slab geometry the temperature behind the front should be of the order of $3 \cdot 10^4\ ^oK$ for $n = 6 \cdot 10^{21}/m^3$, $B_o = 1.6\ W/m^2$, but it is not known what corrections are necessary for cylindrical geometry. The theory also predicts the density to be higher immediately behind the front with a rarefaction wave following behind, but how much mass is moved along with the front in cylindrical geometry is unknown; however, there must be some, and it is likely from the theory that the density in the rarefaction wave is no more than .9 of the unperturbed value. In the narrow region behind the front, there is an axial component of velocity in the direction the front travels, and the mass velocity is approximately 3/8 of the front velocity (or typically 2 cm/μsec).

Another characteristic of this kind of wave is that the current apparently travels down the waveguide on the surface of an imaginary cylinder defined in radius by the outside of the driving electrode. This leaves a hollow "core" where current never flows, so that it might be expected that the degree of ionization and the temperature would be low there. Studies at Berkeley, however, using this same ionizing wave in the same geometry, have shown spectroscopically that in the "core" the ion density is at least 80% of that in the annulus and the temperature > 50% that of the remainder of the plasma (17).

When the ionizing wave reaches the probe, the line is crowbarred so that current running up the alumina probe sheath does not add too much impurity to the plasma from the sheath itself. The crowbar also stops the $\underset{\sim}{E} \times \underset{\sim}{B}_o$ rotation, but not the axial velocity drift, so the plasma drifts to the loop after crowbar in about 10 μsec. It is customary to let the current drive the front a little past the probe sheath and then to wait 10 μsec so that the loop is enveloped in plasma.

The crowbar, in stopping the $\underset{\sim}{E} \times \underset{\sim}{B}_o$ rotation, sets up turbulence in the plasma. The effect of the crowbar is to set

$$\int_0^a E_r dr = 0 \qquad (3.1)$$

but this does not demand that $E_r = 0$ everywhere, so that some motion can still ensue. The severity of the turbulence, as well as its decay in time may be seen in Figure 6.

In view of the turbulence and the "hollow core", the other probable sources of plasma non-uniformity are relatively minor. The

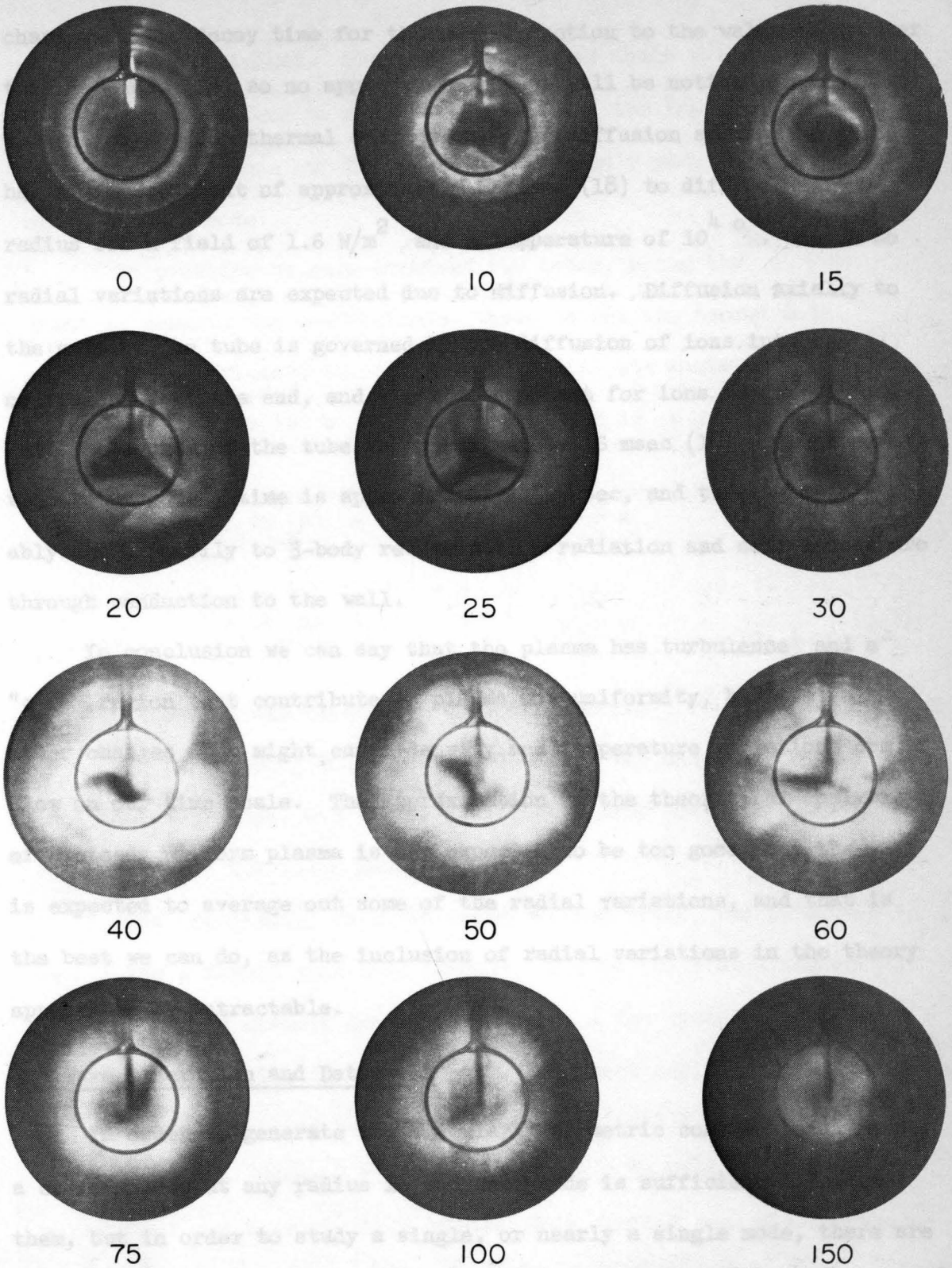

Fig. 6. Kerr Camera Photographs of the Decaying Plasma

The time in μsec after crowbar is indicated below each picture. The shutter time for the first six pictures was .2 μsec, and 1 μsec for the others.

characteristic decay time for thermal conduction to the walls is greater than 300 μsec (18) so no appreciable effect will be noticed in the first 50 μsec or so from thermal conduction. The diffusion across the field has a time constant of approximately 25 msec (18) to diffuse one tube radius for a field of 1.6 W/m^2 and a temperature of 10^4 °. Hence no radial variations are expected due to diffusion. Diffusion axially to the ends of the tube is governed by the diffusion of ions into the neutral atoms at the end, and the time constant for ions to diffuse one-half the length of the tube is approximately 16 msec (18). The over-all temperature decay time is approximately 150 μsec, and this loss is probably due primarily to 3-body recombination radiation and some losses are through conduction to the wall.

In conclusion we can say that the plasma has turbulence and a "core" region that contribute to plasma non-uniformity, but that all other changes that might cause density and temperature variations are slow on our time scale. The approximation in the theoretical analysis of a steady uniform plasma is not expected to be too good, but the wave is expected to average out some of the radial variations, and that is the best we can do, as the inclusion of radial variations in the theory appears to be intractable.

3. Wave Generation and Detection

In order to generate the circularly symmetric compressional modes, a current loop at any radius in the waveguide is sufficient to excite them, but in order to study a single, or nearly a single mode, there are optimum sizes for the loop. In order to excite primarily the lowest mode, we may set the loop size so that the next higher mode has a zero

excitation coefficient. The third and higher modes will then be excited but they tend to damp out faster, and the frequency band below the third mode cutoff will give relatively pure information on the lowest mode.

In practice we have examined two cases, using the $\epsilon_3 \to \infty$ limit to compute the coefficients, where we set the second mode excitation coefficient to (i) zero; and (ii) its maximum value. If the loop radius is b and the tube radius is a, this leads to

$$\text{(i)} \qquad J_1(T_{12}b) = 0 \quad \Rightarrow \quad b = \frac{3.83}{7.01}\, a \qquad (3.2)$$

$$\text{(ii)} \qquad J_1'(T_{12}b) = 0 \quad \Rightarrow \quad b = \frac{1.84}{7.01}\, a \quad . \qquad (3.3)$$

Most of the data was taken with a loop of radius 3.77 cm, approximating condition (i) which yields 3.69 cm. The loop was made of a copper wire in a glass envelope, and the leads left the loop coaxially and went coaxially into the pulse generator.

The experiment, as first conceived and tried, was to excite a wave using a damped sine wave current. Due to the plasma impedance, however, the LC circuit damped to $1/e$ in a few cycles, and rapid damping coupled with the dispersion made direct analysis very difficult. We then tried exciting the plasma with a critically damped sine wave circuit with an undamped frequency of about 7 megacycles, so that the pulse width was approximately 40 nsec. This excited some of all frequencies and the full dispersion of the plasma became apparent in the received signals. The analysis was not extremely simple, since all the frequency

information was there, but the analysis of the received signal yielded the entire dispersion relation on a single shot over the frequency band excited by the pulse.

This technique is discussed at length in the next section.

The pulse itself was produced by a .002 μfd capacitor charged to 14 kv and discharged through a 22 ohm 2-watt carbon resistor by a spark gap into the loop. Although the peak power through the resistor was more than 10^4 times the rated power, only 2 joules were dumped into the resistor, and no ill effects were observed after thousands of firings. While the loop was imbedded in the plasma, the plasma added some additional impedance, which was frequency dependent, so the circuit was somewhat overdamped; but the important thing was that the waveform of the pulse could not be described by a simple RLC circuit, and for the wave analysis, the actual waveform was measured for comparison with the received signals.

The signals were detected with 10-turn magnetic probes which had a measured response which was essentially flat to 15 megacycles and down 3 db at about 22 megacycles. They were constructed inside a piece of slotted solid-wall 50-ohm coaxial line. The signal was fed through a high pass filter into a Tektronix 555 dual beam oscilloscope. Filters were necessary to eliminate pickup from the slowly changing axial field and also to eliminate any slow changes in the plasma after crowbar. The filters cut off charply at about .5 megacycles and their entire frequency response to 50 megacycles, in conjunction with the probe and the oscilloscope was measured and calibrated; although, as we shall show in the next section, we do not need to know this information for the final data analysis.

The probes were inserted into the plasma inside alumina sheaths which extended radially beyond the center of the tube far enough so that the sensitive area of the probe could be placed on axis. These sheaths could be placed every 10 cm down the length of the tube, but it was found that best results in the way of plasma uniformity were obtained with one sheath placed 20 cm upstream from the loop, with both pieces lying in the central region of the tube so as to be far from end effects and reflections.

For timing reference a probe was inserted into the pulse generator and sampled the field due to the pulse current. This signal was always displayed on the upper beam of the dual beam oscilloscope and served to define zero time.

The two traces, the pulse and the signal from 20 cm away, were photographed on Polaroid film and all wave analysis was done from the photographs.

4. Data Analysis Technique

If one were to excite the plasma with a true delta function of current, and record the received signal with no distortion at all, then the Fourier transform of the received signal would yield the transfer function of the plasma by definition. This transfer function could be related theoretically with the dispersion relation itself, although here we always compared the theoretical and experimental transfer function rather than the dispersion relation itself. If the excitation coefficient were independent of frequency, then the transfer function would be simply related to the dispersion relation by a constant. To find the theoretical transfer function, we note from 2.52 and 2.53 that

the axial wave magnetic field transform on axis is given by

$$b_z(\omega,z) = \frac{\mu_o I_o b\, \mathcal{E}_\theta(b)(1+\tau)\, e^{-ikz}}{2\int_0^a (\mathcal{E}_r \mathcal{H}_\theta + \mathcal{E}_\theta \mathcal{H}_r) r dr} \tag{3.4}$$

for the compressional mode. Now a general response is expressed in terms of a forcing function, in this case the current transform times the transfer function, so we may write

$$b_z(\omega,z) = I_o(\omega)\, T(\omega,z) \tag{3.5}$$

where now

$$T(\omega,z) \equiv \frac{\mu_o b\, \mathcal{E}_\theta(b)\, e^{-ikz}}{2\int_0^a (\mathcal{E}_r \mathcal{H}_\theta + \mathcal{E}_\theta \mathcal{H}_r) r dr}, \tag{3.6}$$

But we always examine the signal from a magnetic probe, and hence the derivative of the wave field. This means that we write for the Fourier transform simply

$$\dot{b}_z(\omega,z) = i\omega b_z(\omega,z) = i\omega I_o(\omega)\, T(\omega,z) \quad . \tag{3.7}$$

However, we always observe the forcing function, the current, also with magnetic probes, so we can write

$$\dot{b}_z(\omega,z) = \dot{I}_o(\omega)\, T(\omega,z) \quad . \tag{3.8}$$

since

$$\dot{I}_o(\omega) = i\omega\, I_o(\omega) \quad . \tag{3.9}$$

We now notice that we never observe the true fields, inasmuch as we use a magnetic probe which has a non-flat sensitivity over the frequency range considered, and we also use a high pass filter in conjunction with the oscilloscope. The detecting system might be represented by another transfer function which, for the signal receiving system we might call H_1, and for the current pulse measuring system we will call H_2. Then we have

$$\dot{b}_z^*(\omega,z) = H_1(\omega)\,\dot{b}_z(\omega,z) \tag{3.10}$$

and

$$\dot{I}_o^*(\omega) = H_2(\omega)\,\dot{I}_o(\omega) \tag{3.11}$$

where the * denotes the actual measured quantity. Using equations 3.10 and 3.8 we may now write

$$\dot{b}_z^*(\omega,z) = H_1(\omega)\,\dot{I}_o(\omega)\,T(\omega,z) \tag{3.12}$$

and using 3.11 we may further write

$$\dot{b}_z^*(\omega,z) = \frac{H_1(\omega)}{H_2(\omega)}\,\dot{I}_o^*(\omega)\,T(\omega,z) \quad . \tag{3.13}$$

If the systems are now arranged so that

$$H_1(\omega) = H_2(\omega) \quad , \tag{3.14}$$

we may find the true transfer function $T(\omega,z)$ from

$$T(\omega,z) = \frac{\dot{b}_z^*(\omega,z)}{\dot{I}^*(\omega)} \quad . \tag{3.15}$$

In the experiment, condition 3.14 is satisfied by measuring the driving current waveform with the signal receiving system, characterized by $H_1(\omega)$, one time for taking the Fourier transform. It was observed that the shape of the driving pulse was very highly repeatable, so that one measurement was sufficient. After this single shot was taken, the pulse signal was transferred back to the system characterized by $H_2(\omega)$ but only the time of the beginning of the pulse was read from this system, so that any dissimilarities in the systems were unimportant.

At this point we wish to note that all data was taken at $z = 20$ cm , so that although the transfer function was z-dependent, we only studied its frequency dependence; therefore the z-dependence will not be explicitly included from this point on in the analysis.

We may now separate all the quantities in 3.15 into an amplitude and phase, and it is convenient to represent them in exponential form so that

$$\dot{b}_z^*(\omega) \equiv e^{\alpha_s(\omega) + i\phi_s(\omega)} \tag{3.16a}$$

$$\dot{I}^*(\omega) \equiv e^{\alpha_p(\omega) + i\phi_p(\omega)} \tag{3.16b}$$

$$T(\omega) = e^{\alpha_T(\omega) + i\phi_T(\omega)} \tag{3.16c}$$

where the subscripts represent the signal, pulse, and transfer function, respectively. Using these definitions with 3.15 we have, taking logarithms,

$$\alpha_T = \alpha_s - \alpha_p \tag{3.17a}$$

$$\phi_T = \phi_s - \phi_p \quad . \tag{3.17b}$$

Equations 3.17ab supply the recipe for comparing the theory with experiment, for we may take the Fourier transforms of the pulse and signal waveforms (the α_s and α_p are the logarithms of the amplitudes of the transforms of the time functions) on the computer and also compute the theoretical transfer function.

In practice we have made the actual comparison of theory with experiment with two different assumptions. Since system H_1 was used in a different geometry for measuring the current, a relative amplitude calibration was necessary although the frequency dependence was identical. Since a chance of a systematic error at this point existed, we analyzed the data assuming first that our calibration was correct, and then that we had no knowledge of the calibration, and the comparison was only relative for the amplitude data. This latter approach allows also for a possible constant factor error in the amplitude of the excitation coefficient.

In order to make the comparison in the time domain, we observe that from 3.15

$$\dot{b}_z^*(\omega,z) = \dot{I}_o^*(\omega)\ T(\omega,z) \tag{3.18}$$

so that the time function is given by

$$\dot{b}_z^*(t,z) = \int_{-\infty}^{\infty} \dot{b}_z^*(\omega,z)\ e^{i\omega t}\ \frac{d\omega}{2\pi}$$

$$\int_{-\infty}^{\infty} \dot{I}_o^*(\omega)\ T(\omega,z)\ e^{i\omega t}\ \frac{d\omega}{2\pi} \tag{3.19}$$

and we see that the observed pulse transform is used for this comparison.

Due to the complexity of $T(\omega,z)$, the integral is done by Simpson's rule integration on the 7090 computer.

In the formation of the plasma there are three fundamental parameters of the problem which we do not know on any run. These are the percent ionization, the resistivity, and the ion-neutral collision frequency. On the other hand, we presume that we do know the magnetic field strength, the total number density of particles, and all dimensions in the system. Hence we have treated γ, ν, and η, the percent ionization, ion-neutral collision frequency, and resistivity respectively, as disposable parameters, and have attempted to determine them by curve fitting.

Due to the complexity of the computation of the transfer function, the curve fitting was always done by sampling the experimental curves at about ten frequencies, computing the theoretical values at those frequencies, and measuring the absolute value of the differences at each frequency. A weighted average of these differences was taken to be a measure of the quality of the fit.

The procedure of searching for the best fit, as measured by the minimum average error, was to vary one parameter at a time, and find its relative minimum. We always chose to determine γ first, holding the other parameters fixed; then to vary ν, holding γ and η fixed; then to vary η, holding γ and ν fixed. For each parameter a relative minimum would be determined (within 1% in γ and 10% in ν and η) before varying the next one, and the process was recycled until a simultaneous minimum for all three was found. At this point the

tolerance on ν and η was tightened to 2% and again the process was repeated until a simultaneous minimum was obtained. The values of γ, ν, and η thus calculated are within 1% or 2% of the values which give the best fit in the sense described above. This does not guarantee that the accuracy of these values is within this tolerance, because some systematic errors in either the theory or the experiment, and in the method of weighting the various differences could all affect the results in a systematic but unknown way.

It is possible, however, to make some estimates of the relative probable errors of the various parameters by examining the relative increase of the average error incurred by changing each parameter one percent. This gives a measure of the relative curvature of the error curve for each of the three parameters, where a higher curvature means minimum is known better or that the technique is very sensitive to that parameter. A low curvature would imply that nearly any neighboring value would be nearly as good, so that the errors could be much larger.

The method of weighting the differences between the experimental and theoretical values of the propagation and attenuation constants has been used in a systematic way, but the scheme developed involves certain arbitrary decisions which may be open to question. The technique has incorporated some of the knowledge we have about the probable errors in the data recording and reduction, and it is described in Appendix B. A discussion of these errors upon which the weighting scheme is based, follows below.

The technique of obtaining Fourier transforms from a photograph using a digital computer involves several inherent errors. In the first place the photograph only covers a finite time period, so that ignoring

the portion of the signal which is left off introduces some error. The general treatment of the error introduced by truncation is included in Appendix A and the result may be summarized as a "smoothing" of the transform if any information is really chopped off. A more specific approach to the error in our particular problem is also treated, using the knowledge of the asymptotic form of the time waveform, and this result shows that the error in our case is principally near the cutoff frequency, and the maximum error in the amplitude of the transform is directly related to the amplitude of the function at the time of truncation. The resulting maximum error may be expressed as

$$\text{Max.Error} \approx \frac{\tau}{2} \cdot (\text{amplitude of function at trunc.point}) \qquad (3.20)$$

where τ is the exponential decay time constant. This result is only approximate, since the function only approximately resembles a damped sine wave at long times.

Another error results from computing the transform by a digital method, i.e., the function is sampled at only a finite number of points. In Appendix A it is shown that if any appreciable energy is present in the "true" transform above a frequency $\omega_N = \pi/\Delta t$ where Δt is the spacing between sample points, aliasing will occur, whereby information at $\Delta\omega$ above ω_N will appear added to the information $\Delta\omega$ below ω_N. We have made Δt small enough, or ω_N high enough that no significant errors should enter our analysis from this source.

A third error results from errors in reading the value of the function at the sample points. In Appendix A the error in the

transform due to this reading error is worked out on the assumption that the errors are uncorrelated in time. Although this assumption is not too good, since errors tend to be much greater where the slope is steep, the expression in Appendix A probably gives a lower limit to the error, so that we can tell where the transform data is not significant. We have generally assumed the mean error to be of the order of an oscilloscope trace width. The result is a probable error which is independent of frequency, so that where the amplitude is high, the percent error is small. The error near maximum amplitude is almost always negligible from this source, but below cutoff and at high frequencies, this error is quite severe and effectively limits the range of validity of the results.

Another type of reading error is that due to a kind of jitter in the sampling so that the data points are not truly equally spaced, but have some scatter about some equally spaced points. The assumption that the errors are uncorrelated is probably good here, and on that basis this error has been analyzed in Appendix A and shows again a white noise spectrum whose amplitude now, however, is related to the root mean square of the slope. The magnitude of this error is comparable in general to the additive reading error, and the two combine simply to give an estimate where the data is significant.

CHAPTER IV

EXPERIMENTAL RESULTS

The quantitative experimental results may be expressed in two ways, corresponding to two different methods of data analysis. These quantitative methods are a) the study of the variation of the cutoff frequency with magnetic field and density, and b) the method of forming the Fourier transform of the impulse response and comparing the observed transfer function with a theoretical transfer function. In addition to these quantitative methods we have studied briefly the excitation of higher modes in a qualitative way, and we examined the radial dependence of the wave magnetic field. We shall first examine the application of the first method to some early results which showed very poor agreement with theory and which led to a major redesign of the experimental apparatus.

1. Early Results

When the experiment was first conceived, the design of the apparatus generally favored the least complicated mechanical design consistent with the specific needs for generating the plasma and detecting the waves. Because there were severe mechanical stresses when the magnetic field was pulsed, glass was generally avoided, and hence the probe sheaths were made of teflon instead of alumina and the exciting loop was covered with teflon and epoxy resin instead of glass. The insulating plugs at each end were made of lucite because of its machinability, and faced with glass because it was realized lucite would deteriorate in contact with the plasma; however, the

lucite was inside the vacuum system. Other minor differences existed between the early equipment and the apparatus described in Chapter III, but these seem now to have been the most important.

With this apparatus, the general qualitative form of the received waveforms was about as expected, but the measured value of the cutoff frequency was systematically lower than expected. Since the cutoff frequency ω_o which is given by equations 2.41 is inversely proportional to the square root of the ion mass density, assuming the gas to be fully ionized gives a lower limit to the expected value of ω_o . Because the observed value was even lower than this limiting value, we re-examined some of the assumptions we made in the theory. We considered other reasonable boundary conditions such as that which would be appropriate for an insulating sheath and expect only very small changes would occur and in the wrong direction. We tried to consider the effect of a radially non-uniform density distribution in a qualitative way, and again the effect is to raise the cutoff frequency. Since the cutoff is not perfectly sharp, the last frequency measured is not the true cutoff frequency, but is systematically higher, with the result again tending in the wrong direction to lend an explanation of the observed phenomena. Our conclusion then was that we probably did have an ion mass density as high as our measurements indicated. Since there was not enough hydrogen in the system to account for all of the mass, we supposed that the result indicated the presence of impurities, either in the form of many lighter ions, such as carbon, or relatively fewer heavy complex ions.

We tested this hypothesis in several ways. First we studied the variation of ω_o with the initial pressure of H_2. If the amount of impurity were nearly constant, we would expect little pressure dependence at low pressures, where the H_2 mass would be less than the impurity mass. The result is shown in Figure 7, where it is apparent that there is little pressure dependence. It should be noted that all points should lie either on or above the line indicating the 100% ionized H_2 dependence, whereas nearly all lie below. The results tend to indicate a nearly constant amount of ion mass when the H_2 pressure was varied over a wide range.

A second test was made by studying the propagation of the torsional mode, which was excited by applying a sharp current pulse through the plasma from the driving electrode to the wall of the tube. At low frequencies $(\omega \ll \Omega_c)$ this mode is dispersionless, so that a pulsed excitation will be detected as a pulse downstream. Some broadening does occur due to dissipative effects, and these make the analysis somewhat difficult, but in principle the Alfvén speed may be measured directly from the time delay between the driving and received pulses. A study of the variation of the Alfvén speed measured in this way against the initial H_2 pressure is also plotted in Figure 7, where the scales for the two sets of data for the two modes have been normalized by using the relation

$$\omega_o = T V_A \qquad (4.1)$$

where $T = 3.83/a$, the appropriate value for the lowest mode. It is apparent that the relation 4.1 is obeyed quite well, and that the

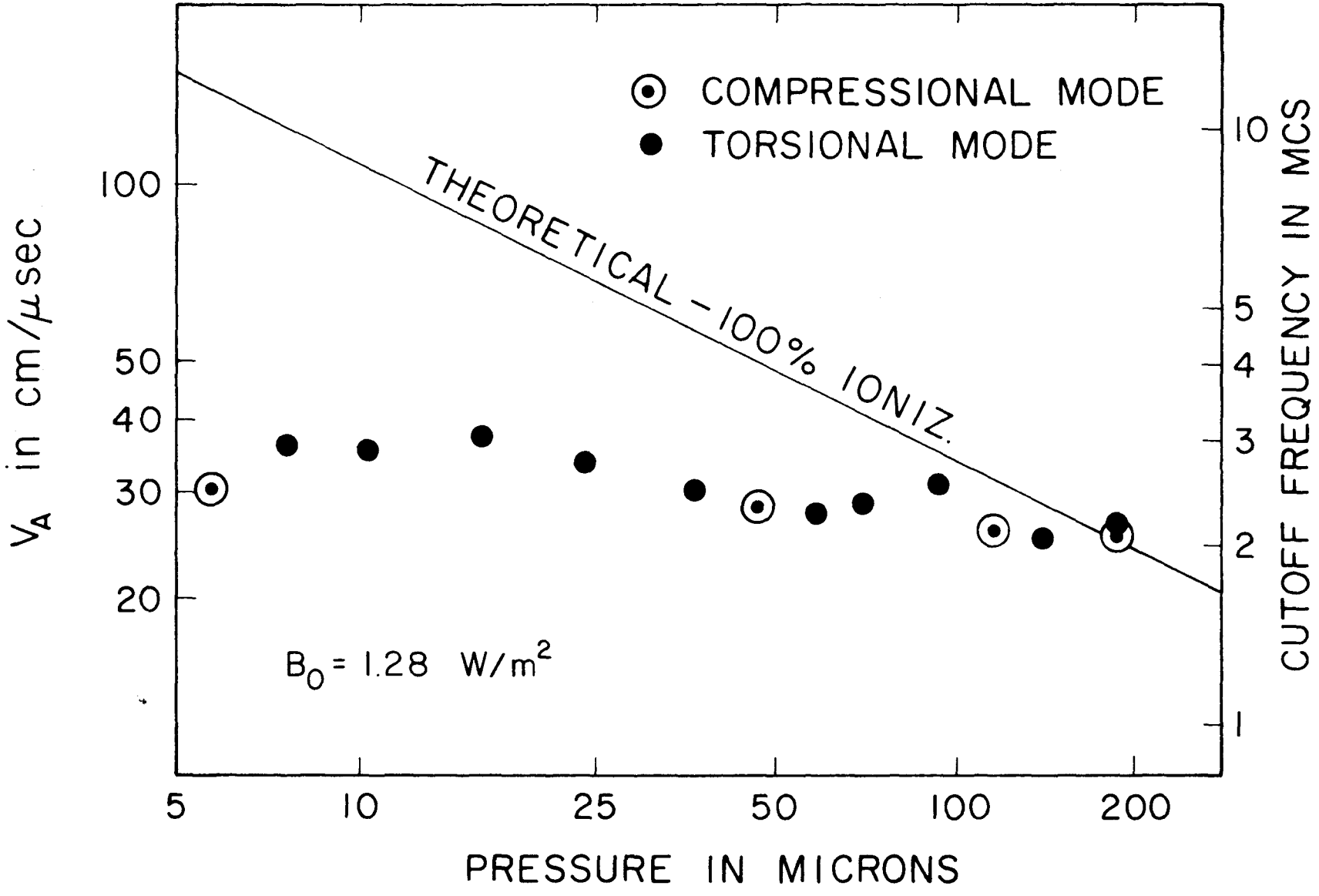

Figure 7. Observed values of cutoff frequency and Alfvén speed versus magnetic field; original apparatus.

torsional mode data shows the pressure dependence to be incorrect but in precisely the same manner as the compressional mode data. This was taken to be rather conclusive evidence that the plasma was seriously contaminated.

A final experiment which was performed inadvertently proved very conclusively that the H_2 made little difference. This experiment occurred when once, quite accidentally, no hydrogen at all was admitted to the chamber, and the experiment proceeded quite as usual. A wave was detected and its cutoff frequency was the same as that for low H_2 pressures. It is significant that a clean system would not even have broken down to form the plasma in the first place, and with the apparatus described in Chapter III, no breakdown will occur with 14 kv on the electrode in the empty tube.

Although the preliminary data was far from ideal, we should note that the relation 4.1 was found to be experimentally verified, and the magnetic field dependence was also verified and found to agree with the behavior implied in 4.1. The result of this study is shown in Figure 8 and the linear dependence of $f_o = \omega_o/2\pi$ upon B_o is apparent. We should also note that the qualitative shape of the received waveforms was in good agreement with those waveforms computed theoretically, except that the time scale was longer, due to the slower Alfven speed.

As a result of these investigations the entire plasma-vacuum chamber was redesigned, along with the solenoid, so that the impurity problem could be minimized. The newer system has no organic compounds

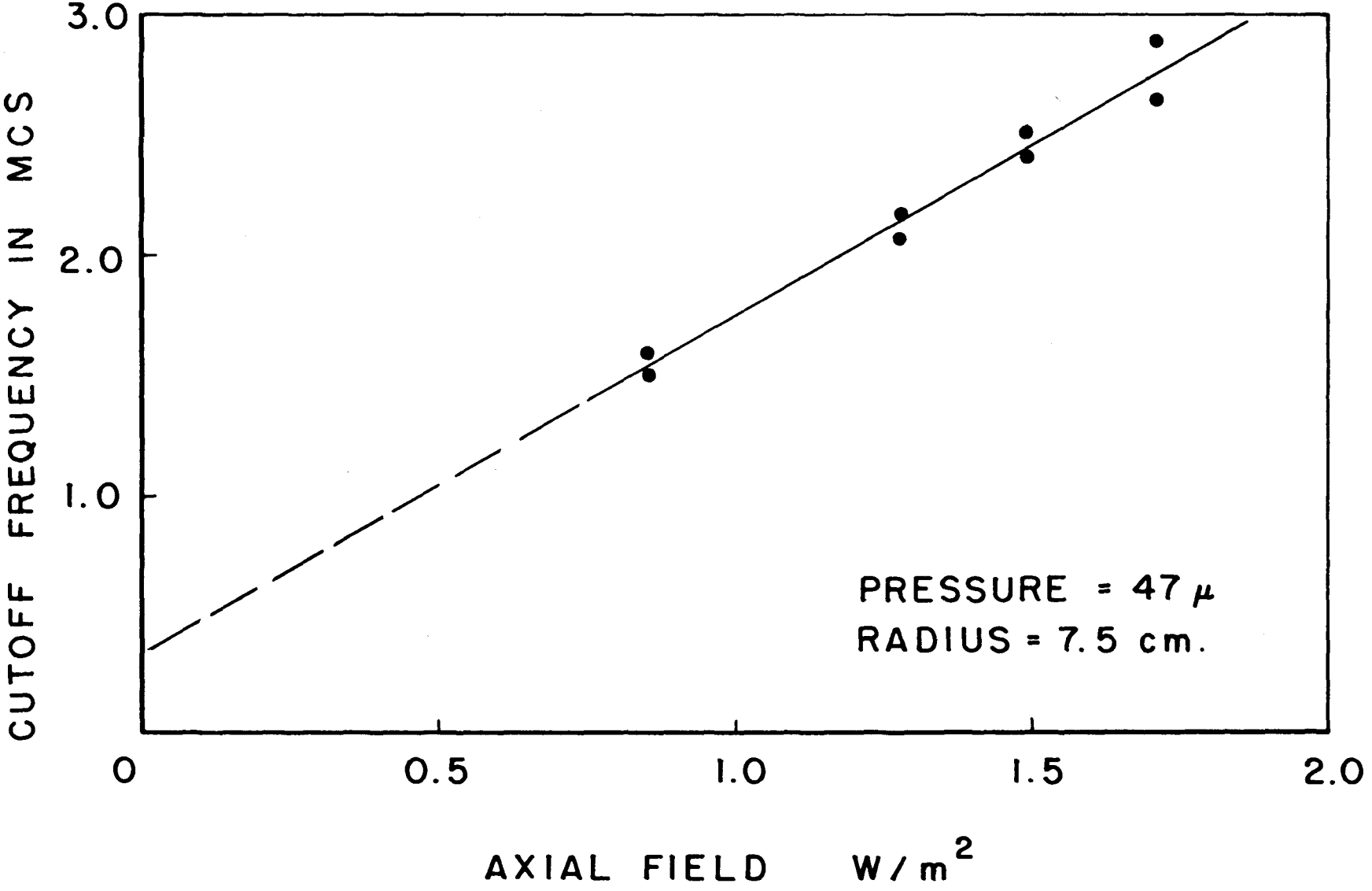

Figure 8. Observed cutoff frequency versus magnetic field; original apparatus

in the vacuum system and only glass, stainless steel and alumina are exposed to the plasma. It is estimated now that the amount of impurity ion mass density is less than the ion mass density of hydrogen when $N_{OH} = 3 \cdot 10^{20}$ m^{-3} (which corresponds to .005 Torr).

2. Studies of the Cutoff Frequency

With the apparatus described in Chapter III which is the updated version of the apparatus in the previous section, the experiments described in that section were repeated. Over 200 pictures were taken at a variety of initial densities and magnetic fields. The data from over 125 pictures were selected for analysis on the basis of the general qualitative features of each picture.

Some pictures showed very irregular waveforms, and some varied in amplitude by large factors from the average value for the particular set of magnetic field and pressure. Most of the irregularities occurred systematically; that is, for a particular setting of field and pressure, ionizing current duration, and delay after crowbar, nearly all pictures were irregular and irreproducible. For a different delay time or ionizing current duration, however, the pictures might tend to be both regular and nearly reproducible with only 10-15% variations in amplitude on a shot to shot basis. The settings of the delay time and ionizing current duration were somewhat critical, in that shortening or lengthening either one by about 5 μsec (but not by 2 μsec) typically would change things noticeably; whereas lengthening the delay time by about 20 μsec or more brought about reproducible signals, although smaller in amplitude.

The irregularities apparently have to do with the location of the ionizing front at the time of the event. If the ionizing current were turned off 5 μsec sooner than usual, the ionizing front might either not arrive at the loop, or just arrive at the loop, and this could give rise to severe irregularities. In the next 5 μsec, however, the loop is certainly imbedded in the plasma, since the front speed is of the order of 5 cm/μsec. If the delay time were too short, again the front might not arrive, as crowbar generally occurred just after the front passed the detecting probe sheath (see Figure 6, frame 1). After crowbar, the front continued to move at about 2 cm/μsec, so again the loop was definitely imbedded in the plasma if the delay was long enough. If the current ran too long, the ionizing front might be driven into the exciting loop, whereas normally it "coasted" the last 10 cm or so. In this case the Kerr cell photographs have shown even more severe turbulence to occur than was shown in Figure 6 and severe contamination was suspected from the probe sheath, since a bright arc was swept out in the rotating plasma. If the delay time was too long, another irregularity occurred in the waveforms. This irregularity did not appear to be correlated with any obvious turbulence as seen by the Kerr cell camera, but possibly had to do with reflections of the wave. This irregular period lasted only 15 to 20 μsec, after which the signal gradually became smaller in the decaying plasma.

Thus a 5 μsec "window" was located for each set of values of pressure and magnetic field which gave a maximum amplitude, qualitatively regular, generally reproducible signal. At the lowest

pressures and highest magnetic fields, this window was very short and some of this data has been discarded because of the irreproducibility. This implies the length of the window has some sort of inverse dependence upon the Alfvén speed, as might be expected, as the over-all time scale is shortened at high Alfvén speeds.

For each of the more than 125 pictures, the last observable frequency was measured, generally by taking an average of the last three or four half-cycles. Measuring the cutoff frequency in this manner introduces a systematic error, for the cutoff frequency is always lower than the last measured frequency for the amount of damping observed in the experiment. The percentage error may be assumed to be nearly constant, however, so that parameter studies will still show the proper trends, but the numerical values will be systematically high.

The results of the parameter study are shown in Figures 9, 10 and 11. Figure 9 shows the dependence of the measured cutoff frequency upon initial density for several magnetic fields. In general, each point represents an average taken from two or three pictures. For the case with the lowest magnetic field, a reference line is drawn in to indicate the value of the cutoff frequency for a 100% ionized plasma.

Several things may be noted from the data of Figure 9. First, it may be seen that there is no apparent tendency for the cutoff frequency to level off at low densities as would be expected if impurities were still a problem. Although the straight lines which are drawn to indicate the general tendency do not have the exact slope which the

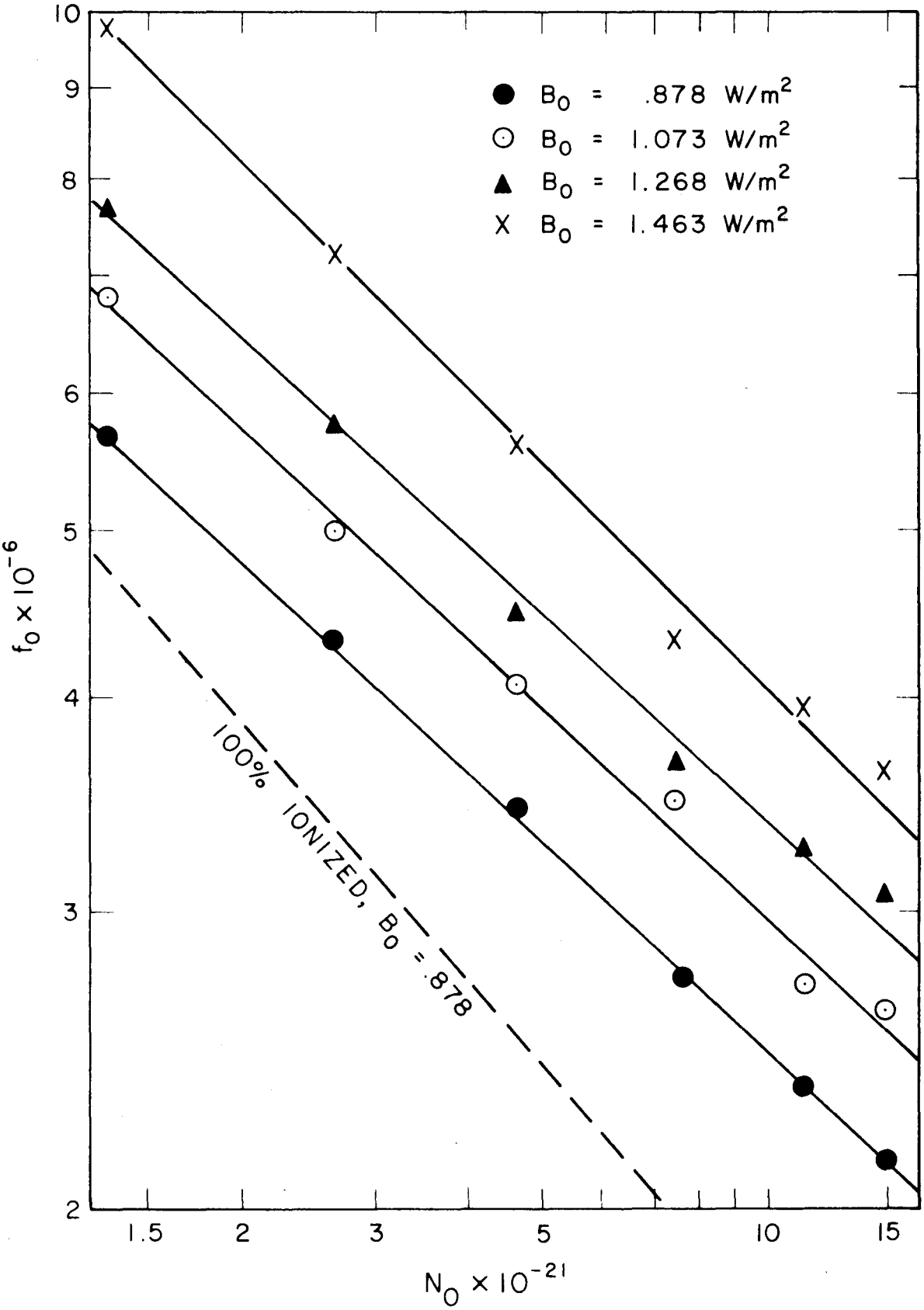

Figure 7. Cutoff frequency vs. initial particle density

reference line has, the points show no systematic tendency to fall below the lines at low densities. From this fact we may estimate that the ion mass density of the impurities, which might be assumed to be approximately independent of the density, must lie well below the ion mass density of hydrogen at the lowest indicated density. We have, in fact, investigated densities even lower than that indicated, and although the results are erratic, we have estimated that the ion mass density of the impurities is probably less than the ion mass density of hydrogen at $n = 3 \cdot 10^{20}\ m^{-3}$ or else the amount of impurities depends nearly linearly upon the hydrogen density.

The second point to notice about Figure 9 is that all of the points lie above the theoretical lines (only the lowest of which is drawn in) which indicate the location of f_o for 100% ionization. This is to be contrasted with Figure 7, where the points nearly all lie below the reference line. This indicates the plasma is generally partially ionized, and although the systematic error involved in reading f_o from the photographs always estimates the percent ionization too low, the result is still true, as the error is always too small to account for all the differences from the 100% ionization reference lines. This error has been estimated by the more careful treatment of some of the data, which is discussed in the next section and it appears that the transfer function analysis generally yields a percent ionization about 6% $\pm$ 10% higher than the measured cutoff frequencies indicate.

The third point to notice is that the slope of the lines which have been drawn through the data points is systematically different

from the slope of the reference line. This indicates a systematic change in percent ionization as the initial density is changed. No such systematic variation with magnetic field was found, so the percent ionizations for the various fields were averaged for each density, and the average value--with the rms deviation indicated with error bars--has been plotted against the logarithm of the density in Figure 10. This graph shows a steadily decreasing percent ionization at higher densities, indicating the ionization mechanism seems to be less effective at higher densities. The ion density does still increase with increasing initial density, but the number of neutrals increases faster. There is no theoretical explanation known for this effect, but the tendency is in the direction one might expect, in that any scheme with a limited amount of potential energy cannot continue indefinitely to ionize all the particles as their number increases. The total energy of the ionizing current bank is at least three times as much as is needed to ionize all the hydrogen and heat it above $10{,}000^{\circ}K$ at the highest density indicated, but still some limiting process may take place.

The fact noted above, that the percent ionization shows no systematic trend with the magnetic field, is illustreated in Figure 11. Here the plot of f_o against the magnetic field shows that a straight line through the origin is as good a fit as one which only comes close. The scatter in the data is large enough that a non-zero intercept could occur. But the average of the data shown, along with other data at different densities, shows that the lines do extrapolate very close to the origin, certainly within the probable error, giving no

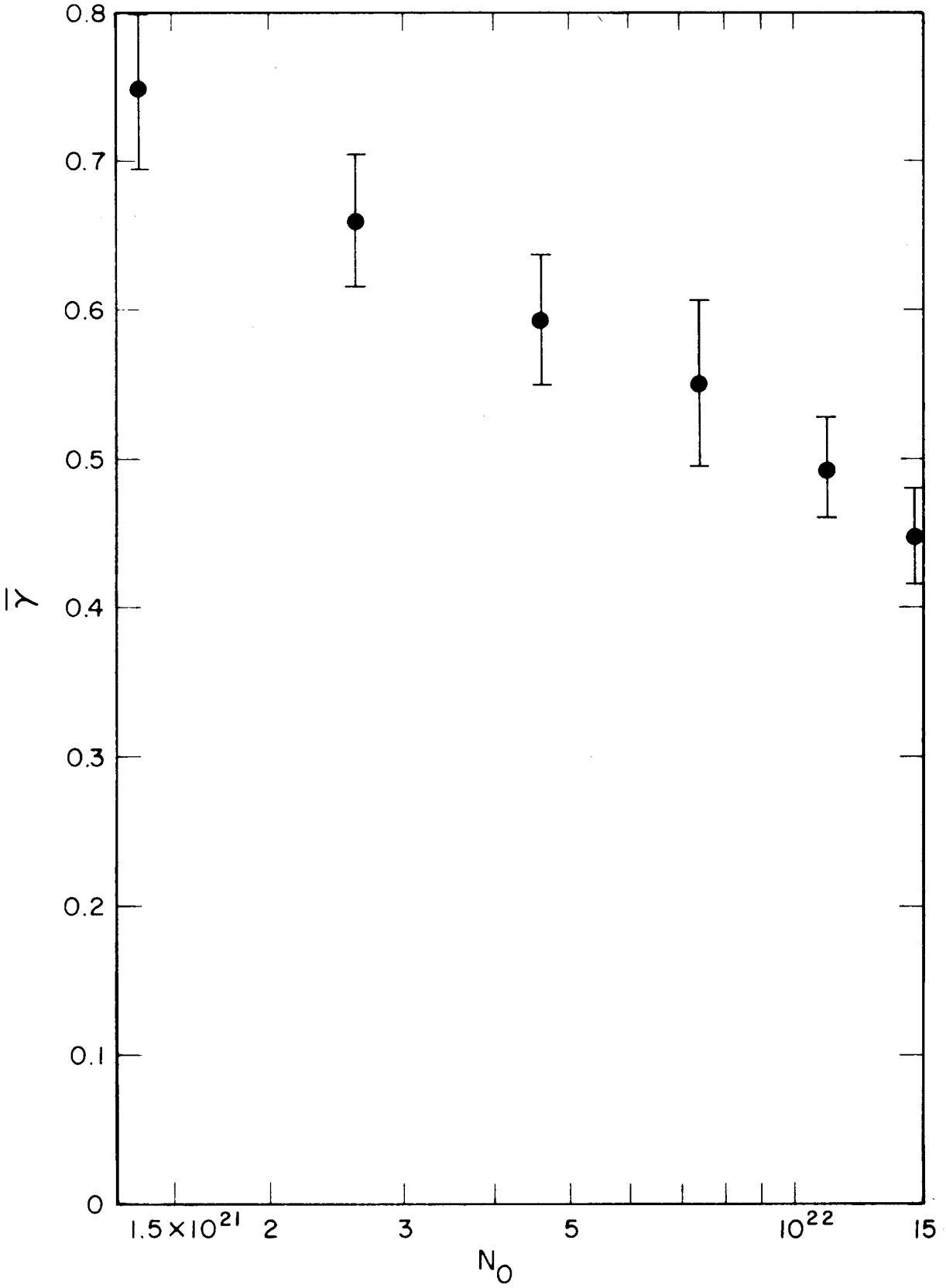

Figure 10. Avg. degree of ionization vs. initial particle density

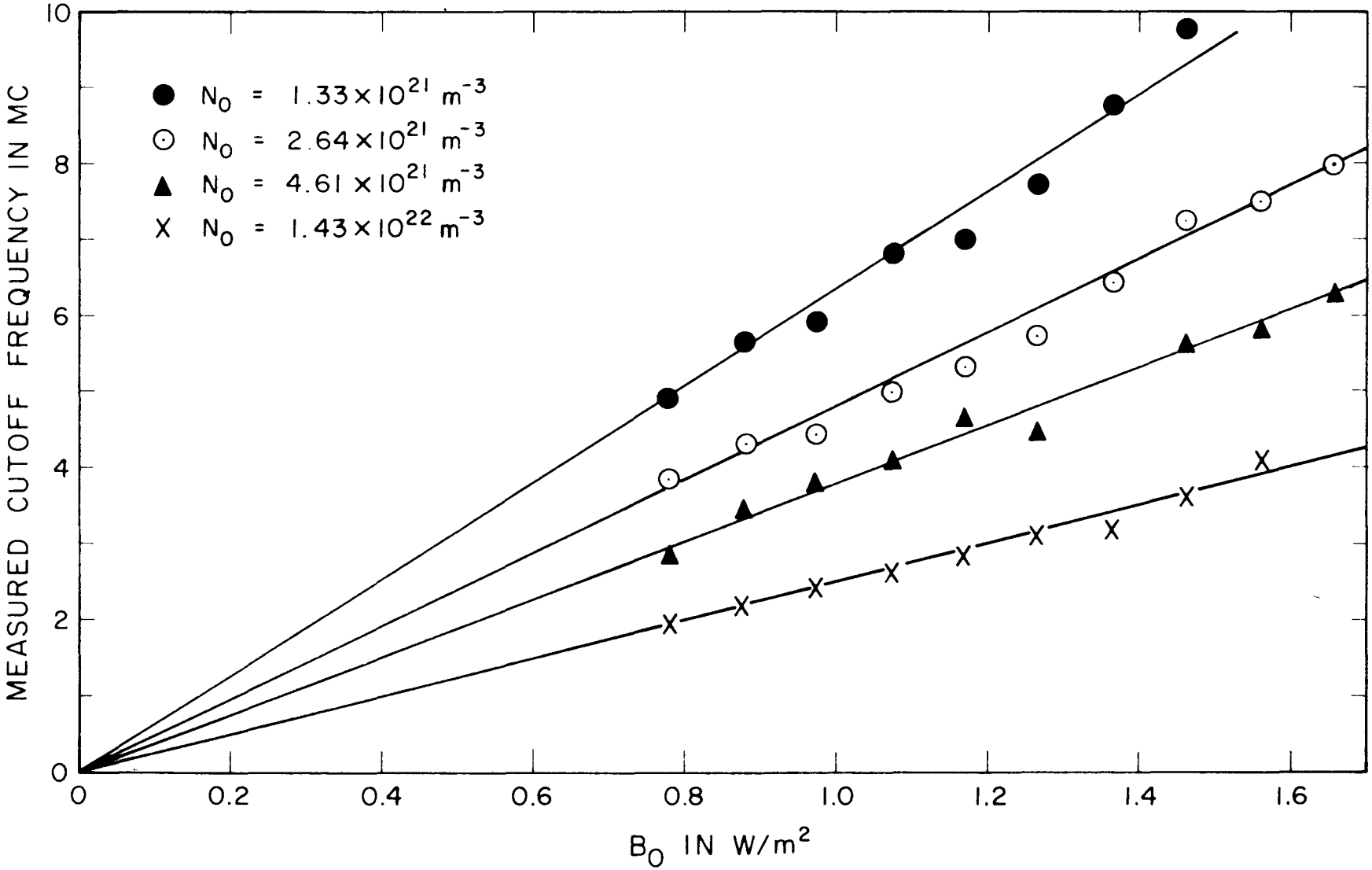

Figure 11. Cutoff Frequency vs. Magnetic Field Strength

evidence of a systematic variation in the percent ionization with the magnetic field. The dependence illustrated in Figure 11 is the same as in Figure 8, except that now the agreement with theory may be made quantitative, assuming a partial ionization, instead of only qualitative as was the best previously possible when all values of f_o were too low.

One apparently obvious check on the cutoff frequency has been omitted in the present analysis of data. Whereas the velocity of the torsional mode was measured in the earlier experiment, and the velocity obtained in this manner compared with the value computed from 4.1, no such comparisons have been made with the more recent data. The reason for this is due to the amount of pulse distortion in the propagation of the torsional wave. Although ideally this mode is non-dispersive, the dissipative mechanisms apparently influence the propagation so strongly that the pulse is greatly distorted--the distortion being primarily a large broadening of the transmitted pulse. It is suspected that the delay between the peaks of the driving and received pulses, or since magnetic probes which detect the time derivative of the field are used, the delay between zero crossings, gives a reasonably good estimate of the Alfvén speed. But the accuracy of such an estimate is not presently known, so we have put this information aside for a separate investigation at a later date.

3. Study of the Impulse Response

The most critical test of the adequacy of the plasma model involves the study of its frequency dependence. This is especially true if the wave propagation is very dispersive as is the case for the compressional mode, particularly near cutoff. There are at least three more or less separate effects which cause dispersion in the frequency range we have chosen to study. First, the boundary condition is responsible for the cutoff phenomenon, so the study of the transfer function in this frequency range will give information about the boundary condition and indicate the adequacy of the theory to describe it.

Second, if the ion-cyclotron frequency lies in the range of frequencies studied, the propagation constant differs significantly from the value it would have if the ion-cyclotron frequency were well above the observed frequency range. With the magnetic field we have available, this critical frequency does lie either in or near the range of frequencies we can study, so the dispersion due to ion-cyclotron effects should be noticeable. Hence we should be able to check the adequacy of the model near this frequency.

Third, the ion-neutral effects should lead to some dispersion in this range, since the ion-neutral collision frequency is comparable generally to the cutoff frequency. The effects are frequency dependent and generally extend into the propagating region above cutoff. We expect that some indication of the adequacy of the method of including ion-neutral effects should be apparent from the data. However, in the experiment the effect is generally small, since the resistive damping

is so large, so the statistical errors in the data may make the comparison with theory less significant than it would be if the resistivity were small.

In order to study the transfer function over a frequency band, a method which gives all the information on a single shot is a great advantage, since our plasma is not, in general, highly reproducible. This was accomplished by exciting the wave with an impulse which was very short compared to the time scale of the received signal. This yielded a spectrum which was nearly flat over the frequency band from below cutoff to the upper limit of the range of the detection equipment. The actual shape of the impulse was measured and from its Fourier transform we were able to normalize the transform of the received signal so that we had the effective response to a delta function (see equation 3.15).

An example of the received waveforms is shown in Figure 12, where the impulse is shown in the upper trace and the received signal below. That the qualitative features are as expected may be seen by comparison with Figure 4 (which was not intended to match Figure 12 quantitatively). Nearly twenty such pictures have been analyzed in detail which cover a variety of magnetic fields and initial densities. Each such signal has been digitized and its Fourier transform computed on a digital computer at one-hundred frequencies spaced about a quarter of a megacycle apart.

The computed transfer function of the signal shown in Figure 12 is shown in Figures 13 and 14 as an example of the type of data which can be extracted from such a picture. Included in Figures 13 and 14

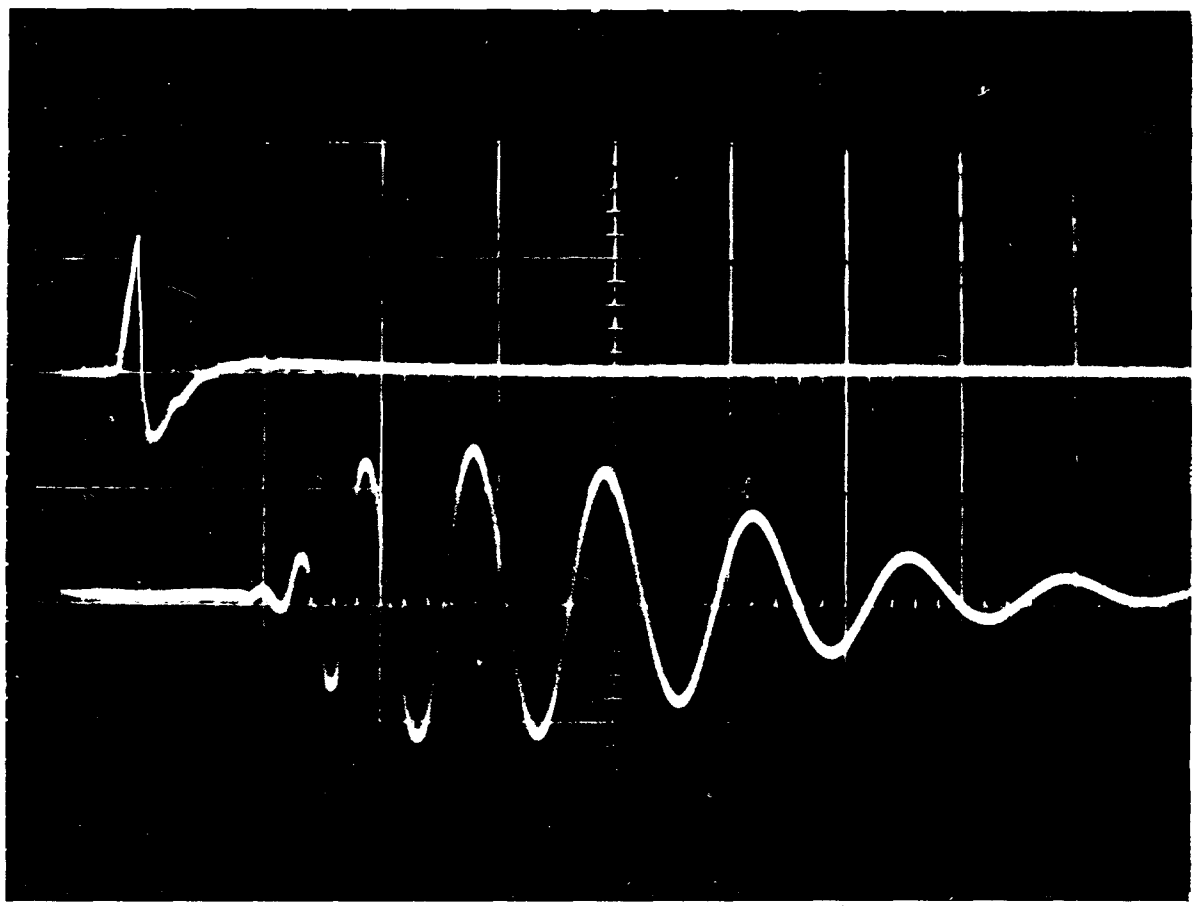

Figure 12. A typical photograph of a received signal. The upper trace is the time derivative of the driving current, as measured with a magnetic probe, and is displayed for timing reference (amplitude arbitrary). The lower waveform is the signal received from a magnetic probe which measures the time derivative of the axial component of the wave magnetic field on axis, 20 cm from the driving loop. The vertical sensitivity for the lower waveform is 20 gauss/μsec/div. The horizontal scale is .2 μsec/div.

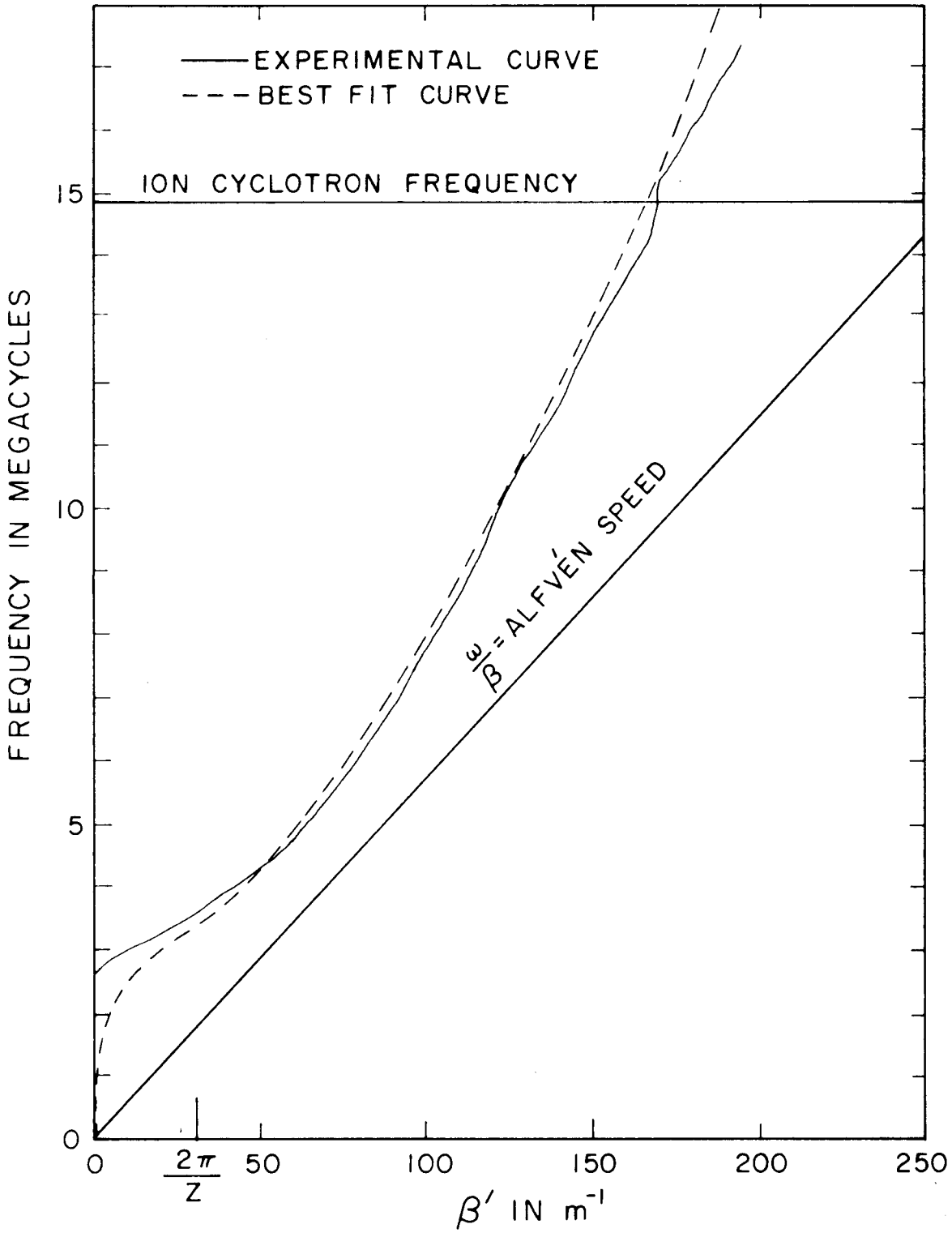

Figure 13. Frequency vs. transfer function effective propagation constant at z = 0.2032 m.

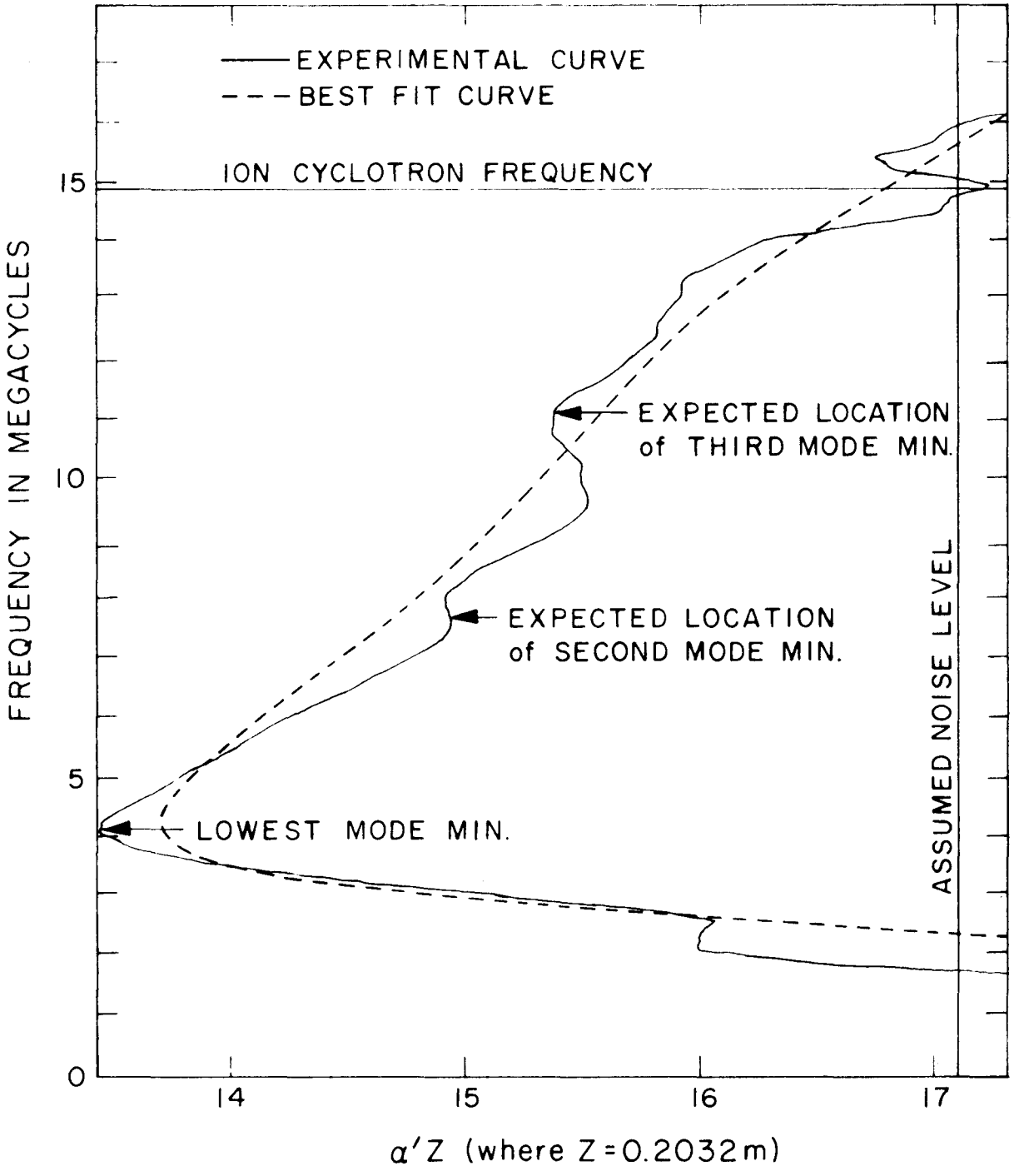

Figure 14. Frequency vs. transfer function effective attenuation constant.

are the theoretical transfer function phase and amplitude curves respectively, which were determined by the curve fitting technique described in Chapter 3. Several characteristic features of the experimental transfer functions may be noted from this example. We observe that the shape of the phase curve generally fits the theoretical curve very well except near and below cutoff and at very high frequencies where the amplitude shows high attenuation.

It is characteristic of the data that the experimental phase curve does not usually bend down near cutoff, but appears to go to a negative phase. It is thought that since the attenuation is changing so rapidly with frequency in this region, and since it is quite high where this phase error occurs, we do not attach too much significance to the apparent discrepancy.

Well below cutoff, the phase is determined only by noise, and is hence random; this makes the origin of the phase curve indeterminable by following it down to zero frequency. The phase is then usually undertermined by some multiple of $2\pi/z$ and often our computer convention of keeping track of the phase as it goes through successive cycles introduces an error of one or two multiples of $2\pi/z$. The number of cycles erroneously introduced by this convention is usually apparent from some general considerations about the shape of the curves, and an experienced eye can nearly always guess immediately where the proper origin belongs and correct the error. If an improper choice is made, however, the curve fitting technique yields highly doubtful values for the adjusted parameters, and the least average error is often five times as high as it is for the proper choice. This has

been tested in several cases where the phase origin was deliberately offset by $2\pi/z$ in both directions from the presumed origin, with the result that the alternate choices gave either ridiculous or highly doubtful values for the parameters, and the fit was invariably much worse. Occasionally a wrong choice has been made initially, but the resulting parameter values were so suspicious that the origin was shifted by one cycle and the fit was vastly improved, the best fit values being then quite reasonable. Hence we feel that this ambiguity has always been resolved successfully.

The second general feature is that at very high frequencies, some definite deviations from a smooth curve occur, which appear to be random in nature, or at least to show no trend from picture to picture. In the example shown in Figure 13 the curve exhibited a violent bend toward larger values of β at a frequency just above the highest shown on the graph. At this frequency the indicated amplitude was far below the probable noise level, so this was not included in the figure. It is characteristic of the data that whenever the amplitude is above the noise level, the phase curves match the theoretical curves very closely with no large deviations; but often they deviate greatly when the amplitude is below a few percent of the maximum amplitude.

The frequency dependence of the portion of the transfer function is shown in Figure 14 in terms of the effective attenuation coefficient at 20.32 cm. It should be noted that the effective attenuation coefficient has information about the amplitude of the excitation coefficient so that if

$$b(z,\omega) = b_o(\omega)\, e^{i\omega t - i\beta z - \alpha z} \qquad (4.2)$$

then the effective attenuation coefficient is defined by

$$b(\omega,z) = e^{i\omega t - i\beta' z - \alpha' z} \tag{4.3}$$

so we have

$$\alpha' = \alpha - \log(|b_o|)/z \tag{4.4}$$

such that the α' shown in Figure 14 is z-dependent. This combination is used for comparison because it is the experimentally observed quantity corresponding to the transfer function. Since we did not study the z-dependence of the transfer function, we may treat α' as if it were only frequency dependent.

Several things are immediately apparent from Figure 14. First, the over-all fit is not nearly as good as it was for the phase curve, and this is a general characteristic among the cases we have studied. We may expect then that the determinations of the resistivity and the ion-neutral collision frequency, which are principally determined from the wave attenuation coefficient, will have a larger probable error than the determination of the degree of ionization which is determined principally from the phase information.

Some of the differences between the experimental and best fit curves appear to be systematic and appear to indicate some inadequacy of the theory. First we note that there appear to be indications of higher order modes, and this is a characteristic result in the cases we have analyzed. However, the best fit curves do not usually show much influence from these higher modes, although they would appear more

strongly if the resistivity were lower. If a curve were drawn in corresponding to a lower resistivity, the qualitative features of lower attenuation near the third mode minimum and the sharp increase in attenuation just above that, which is due to interference between the first and third modes, may be recovered. But the basic slope of the curve above the lowest mode minimum would increase in that case and the minimum attenuation would be lower than the experimental minimum. The result of this change would be that nearly the entire curve would lie to the left of the experimental data, and hence yield a poor over-all fit.

It was thought at one time that a much better fit would be obtained if the theoretical curve described above with the proper qualitative features were moved to the right by some appropriate amount. This would correspond to assuming some error in the amplitude calibration of one of the probes. Hence, the entire curve was assumed to be in error by an additive constant, and this constant was treated as another disposable parameter. The result was that the shift was generally small and the average error was reduced somewhat. The best fit values of the resistivity and the ion-neutral collision frequency determined in this way were only very slightly changed, however, so the approach was abandoned with the conclusion that the values were determined principally by the shape of the curve.

There is some evidence that the values obtained for ν and/or η are too high, corresponding to too much dissipation, since if the inverse Fourier transform of the best fit transfer function is taken to produce a time function, the amplitude of the theoretical signal is

systematically lower than the amplitude of the experimental signal, and the envelope indicates a higher damping rate than is observed. Thus if the curve fitting had been done in the time domain, the results might have been systematically different although not by a large amount.

It was mentioned previously that if the resistivity were lowered below its best fit value, effects due to the third mode would begin to appear. However, we would not expect effects from the second mode to appear, since the exciting loop radius was chosen to excite none of that mode. But the experimental results show an effect in Figure 14 and in many of the cases studied which appears to be due to the second mode. We have taken this to be possible evidence of some degree of radial non-uniformity in the plasma, since the cutoff frequency seems to support our assumption about the boundary condition. Only an improper assumption about the boundary condition could account for such large excitation of that mode in a uniform plasma. It is not known how to use this information to make any estimate of the degree of non-uniformity, since consideration of nearly any non-uniform distribution leads to severe computational problems in a cylindrical waveguide. The radial non-uniformity (and perhaps also a longitudinal non-uniformity) in plasma density may also account partially for the discrepancies noted above in the values of η and ν .

When the over-all results from the curve fitting were examined, only one systematic variation with magnetic field was observed. It was noticed that the resistivity appeared to be almost proportional to the magnetic field strength over the range we examined. The results are

shown in Figure 15. The error bars on the points are not to be interpreted as indicating our estimate of the probable error at each point except in a relative sense. Where the error bars are greater, the uncertainty is probably greater. They were deduced from the error curvature near the minimum average error and represent approximately the range over which η must be varied to double the average error, holding γ and ν constant. A possible interpretation of this result is offered in the next chapter.

In general, the degree of ionization determinations showed the least probable error. In some cases the fit was so good that a change in γ of only 2-1/2 to 3% would double the average error, and the average change necessary to produce this result was less than 5%, so the uncertainty in γ is generally small.*

It is worth while to note that the percent ionization computed by curve fitting was 6% higher on the average than the value determined from the measured cutoff frequency. The standard deviation of the ratio of the two determinations was 12%, but for the three cases which had the least average error, the best fit value was 4.5% $\pm$ 3% high. This indicates the method of determining the degree of ionization from the cutoff frequency is probably quite good even though it introduces a small systematic error.

The significance of the value of γ determined by curve fitting or by measuring the cutoff frequency is not completely certain, however,

---

*Even the most extreme weighting schemes investigated in computing the average error to be minimized never changed the best fit degree of ionization by an amount greater than the uncertainty listed above.

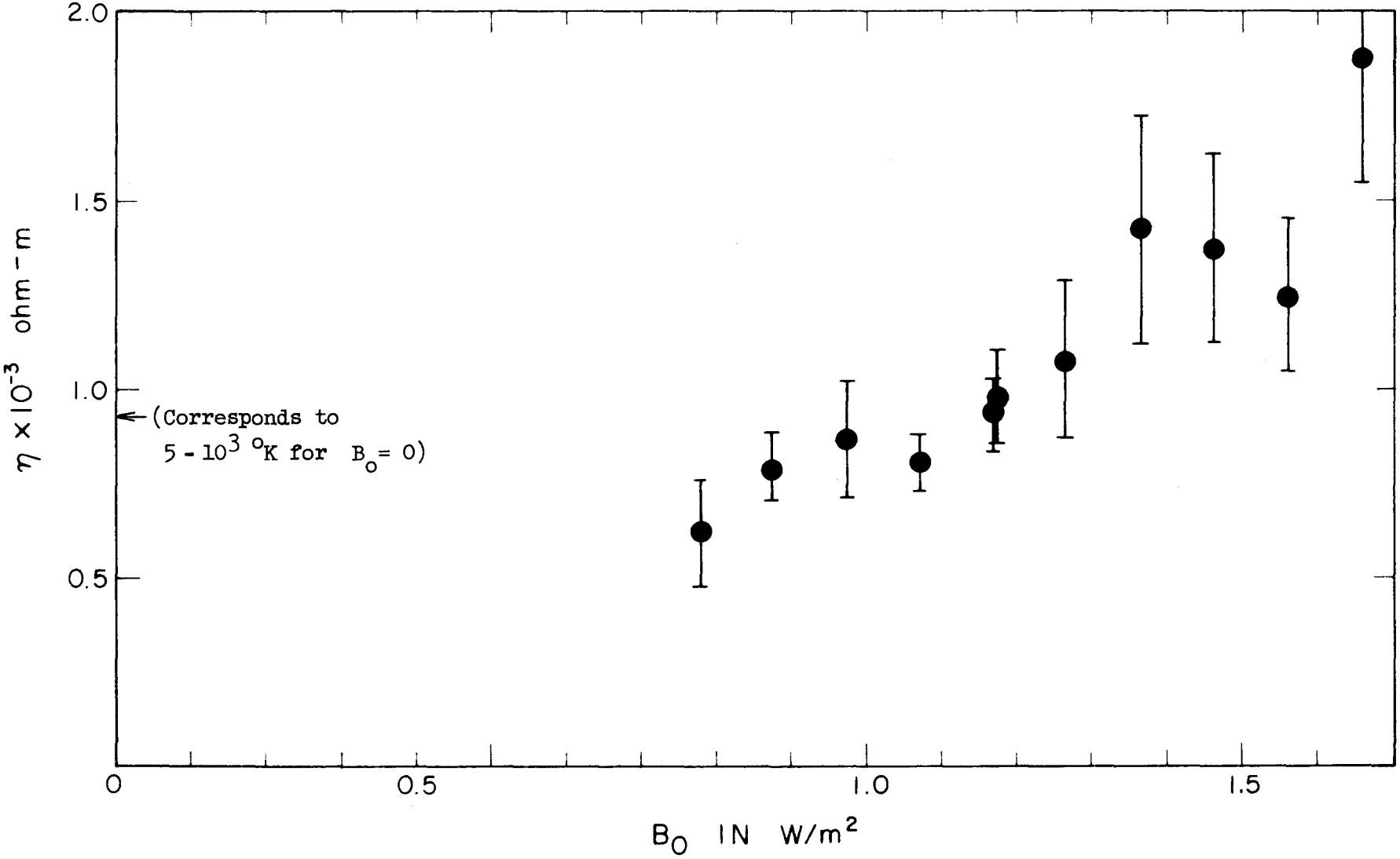

Figure 15. Best Fit Value of η versus B_o

since the plasma is apparently radially non-uniform. Due to the nature of the compressional mode as contrasted with the torsional mode, we expect that the value of γ represents an average degree of ionization over the entire radius. Whereas in the limit of zero resistivity, the torsional mode propagation is determined by the local density along the field lines on which the disturbance was begun, the compressional wave may be thought of as a superposition of waves which travel in all directions at the Alfvén speed. At the cutoff frequency the propagation is only in the transverse direction while the plasma oscillates at a resonance for that direction. When the wave travels only perpendicular to the magnetic field, it is normally called a magneto-acoustic mode, but this is only a special case when the propagation vector is perpendicular to the magnetic field. The compressional mode is defined for propagation only along the field, but the character of the cutoff phenomenon depends upon the superposition of waves going in all directions. Due to this omnidirectional character we expect the value of γ determined by curve fitting to be an average quantity in some sense, but not necessarily the ordinary mean degree of ionization.

The data on the ion-neutral collision frequency taken from the curve fitting technique shows the largest uncertainties as measured by error curvature. The very highest curvature measured indicates that a 9% change would double the error, while some cases indicate that probably a factor of two in the value of ν would only double the error. Since no systematic trends are apparent, we have taken a weighted average of the quantity σv_n where σ is the ion-neutral

cross section and v_n is the neutral thermal speed and we have assumed

$$\nu = \gamma n_o \sigma v_n \quad . \tag{4.5}$$

In the average we have used the error curvature to determine the relative weights, since some values deviate rather widely from the average but have very small corresponding curvature. The result is that $\langle \sigma v_n \rangle = 5.5 \cdot 10^{-15}$ m^3/sec and the probable error is unknown, but the standard deviation is about 20% of this value. The value quoted above is probably of the right order of magnitude, but little is known of the charge-exchange cross-section in this energy range.

4. Other Qualitative Checks

In addition to the quantitative measurements described above, we made a few auxiliary checks of some other aspects of the theory.

After observing some evidence of higher order modes in the measured transfer functions, we used another smaller exciting loop which was designed to excite a maximum amount of the second lowest circularly symmetric mode. Although the effect was not quite as large as expected, a definite difference in the transforms was apparent near the expected minimum of attenuation for that mode. In some cases the interference between modes made obvious changes in the received waveforms, and this tended to distort the pictures so much that even the cutoff frequency was difficult to determine.

The other qualitative check was the measurement of the radial dependence of the axial component of the wave magnetic field. The result

of measuring the amplitude of the signals at different radii with the magnetic probe is shown in Figure 16. The theoretical shape, with the amplitude adjusted, is also shown for reference. The negative amplitudes were determined by a phase reversal of the signals. The large scatter is due to the non-repeatability of the plasma, especially out toward the tube wall. Although the phase was quite regular from picture to picture, indicating the degree of ionization was nearly constant, the amplitude and envelope shape occasionally showed variations as large as 50%, so that the data is only presented to show the basic features. The result is taken as support for the basic assumption about the boundary condition.

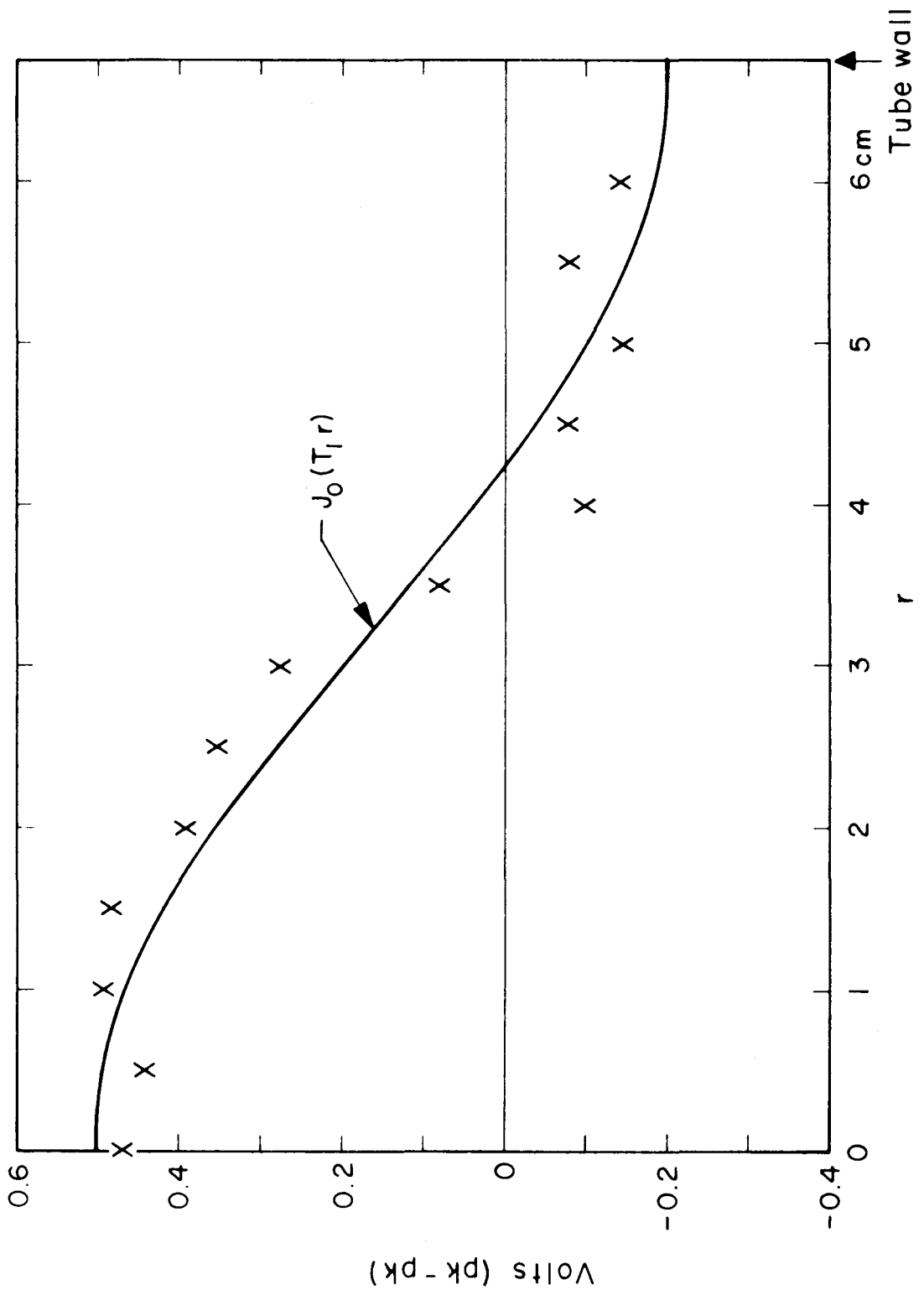

Figure 16. Radial Amplitude Variation

CHAPTER V
CONCLUSIONS

Inasmuch as the plasma is known to be non-uniform, with the degree of non-uniformity undetermined, it is difficult to draw specific conclusions about the adequacy of a theory which is constructed to describe a uniform plasma. In general, however, it is thought that the experimental results indicate that the theory is adequate except perhaps in one area.

It is felt that the general agreement between theoretical and experimental phase curves, such as is evidenced by Figure 13, indicate that the theory adequately describes the dispersion characteristics of the compressional waves in a waveguide within the experimental error. From this type of data the average degree of ionization can probably be determined within 5%.

The more easily determined quantity, the cutoff frequency, gives an accurate enough measure of the Alfvén speed to show its dependence upon magnetic field and density. This method generally indicates a degree of ionization which is low by about 6% with respect to the best fit values with a scatter of $\pm$ 12% .

From the measured value of the cutoff frequency and the characteristic dispersion near it, along with the apparent radial dependence of the axial component of the wave magnetic field, we have concluded that the assumed boundary condition is consistent with the observations. However, these results may be relatively inconclusive as to the exact boundary condition, since the assumption of an insulating sheath surrounding the plasma such that no radial currents are allowed to flow to the wall, may lead to basically the same radial field dependence

and nearly the same value of the transverse wave number.

Since the curve fitting technique was so insensitive in determining the value of the ion-neutral collision frequency with the observed data, it is difficult to make any real estimate of the accuracy of the determinations. There may be systematic trends which exist in the present data but were overlooked due to the scatter in the data. Since it is difficult to measure the charge-exchange cross-section at low energies by alternate methods, this method might be useful in experimentally determining this quantity if the errors could be reduced.

The most significant tendency observed which may indicate an inadequacy in the theory was presented in Chapter IV and shown graphically in Figure 15. This data shows a tendency for the resistivity to increase with magnetic field over the range studied and, although the uncertainties are admittedly large, the trend is believed to be systematic. Several possible explanations may be offered for this phenomenon.

First, the effect may be due to some unknown systematic error in the experimental technique or method of data analysis. We have investigated the possibility of an incorrect amplitude calibration of the magnetic probe as described in the previous chapter, with the conclusion that it could not account for this result since the best fit values of η are determined principally by the slope of the amplitude curves and not by the magnitude of the amplitude. It is possible that some non-uniform density effect could be responsible for the trend, but this is doubted, as we have been unable to understand the effect even qualitatively on this basis.

A second possibility is that the effect may indicate some systematic decrease of temperature with magnetic field, since the classical

resistivity depends approximately inversely on the temperature to the three-halves power. This possibility is also doubted since in the formation of the plasma the temperature both just behind the ionizing front and in the rarefaction wave farther behind, varies as the square of the ionizing front velocity and this velocity increases monotonically with increasing magnetic field (16). It is difficult to understand how that trend could be reversed only 15 μsec after the ionizing wave is turned off. In fact, it is more likely that the temperature varies only slightly if at all with magnetic field, since the percent ionization shows no systematic variation, and some degree of quasi-equilibrium may well have been established.

A third possibility for understanding the trend shown in Figure 15 is that there may be some inadequcy in the theory which assumes that the resistivity is isotropic. We have always assumed η to be a scalar quantity, which implies the resistivity is independent of direction, while the σ tensor, which we shall call the effective conductivity tensor, is not the reciprocal of η but is the description of the conductivity in the laboratory frame, and is not a scalar quantity. Hence we have assumed that the anisotropy of the plasma properties in the laboratory frame are not due to any anisotropy in the momentum transfer due to collisions.

This view is not strictly correct, however, if the electrons make several Larmor rotations about the magnetic field lines between collisions with ions. In such a case, the resistivity does have tensor properties, and the component perpendicular to the magnetic field may be larger than the parallel component by as much as a factor of 1.93

according to a computation of plasma transport coefficients quoted by Bernstein and Trehan (19). The cross-over region between the isotropic and anisotropic cases occurs when the ratio of the electron cyclotron frequency to the electron-ion collision frequency is approximately 1.5 . In the region near this value for the ratio, the transverse resistivity then increases with increasing magnetic field to a value about double its parallel value. From the values of η indicated in Figure 15, the value of this critical ratio appears to change from a value of about 1.5 to 3, so that the trend indicated may be evidence of this cross-over, since the compressional mode depends almost entirely on the transverse resistivity.

If this tentative hypothesis is correct, the trend of Figure 15 should not continue beyond the range indicated, so that lowering the ratio of ω_c to ν_{ei} should not lower the value of η observed very much, and raising the ratio should not raise the upper value very much. Unfortunately, it is difficult to change ω_c much beyond the range indicated with the experimental apparatus at hand. However, the electron-ion collision frequency ν_{ei} is proportional to the electron density, so it is possible that the range of the ratio ω_c/ν_{ei} can be extended and we can discover, whether the trend continues or levels off at a finite limit.

There is data at hand which was taken over a wide range of pressures, but its analysis was not completed in time for this report. This study is being continued and this trend will be examined further over a wider range of the ratio ω_c/ν_{ei} .

Another avenue of investigation which may be pursued is the study of the torsional mode in this same plasma. The damping of this mode depends principally upon the parallel resistivity, so that if the trend of Figure 15 were really due to a variation in temperature η should show the same behavior for the torsional mode. If it is due to the crossover from an isotropic plasma to an anisotropic plasma, however, the value of η measured from the torsional mode should show no such trend in the same region. This could, perhaps, be a critical test to determine the adequacy of the present theory.

APPENDIX A

Errors in Fourier Transforms Computed by Digital Methods

(Adapted from a research note by R. H. Hertel)

In the Fourier analysis of oscillograph records and similar data by digital methods, significant errors may be introduced by the computation process. Four sources of error will be discussed here:

A. Truncation
B. Sampling
C. Additive Noise
D. Timing Jitter

It is assumed that the function $f(t)$ to be analyzed is zero for $t < 0$ and has a Fourier transform $F(\omega)$ given by

$$\mathcal{F}[f(t)] = F(\omega) = \int_{-\infty}^{\infty} e^{-i\omega t} f(t)\, dt \,. \qquad (1)$$

The computed transform $F^*(\omega)$ is to be obtained by truncating $f(t)$ at $t = T$, sampling at $N+1$ uniformly spaced times, and computing the transform of the resultant function. It is assumed that errors may occur both in choosing the sample times and in converting the value of the function to digital form. To simplify the discussion the sources of error listed above will be treated separately.

A. Truncation

Including only the effects of truncation permits us to write for the computed transform

$$F^*(\omega) = \int_{0}^{T} e^{-i\omega t} f(t)\, dt \quad : \qquad (2)$$

No harm will be done if this is rewritten

$$F^*(\omega) = \mathcal{F}[f(t)\ g(t)] = \int_{-\infty}^{\infty} e^{-i\omega t} f(t)\ g(t)\ dt \qquad (3)$$

where

$$g(t) = \begin{cases} 1\ ; & |t| < T \\ 0\ ; & \text{otherwise} \end{cases} . \qquad (4)$$

Thus the effect of truncation is identical to multiplication by $g(t)$. No change would be introduced by making $g(t)$ zero for negative times since $f(t)$ is zero there anyway; the choice made here is in the interest of simplicity in the results. Now multiplication in the time domain corresponds to convolution in the frequency domain:

$$\mathcal{F}[f(t)\ g(t)] = \int_{-\infty}^{\infty} F(x)\ G(\omega - x)\ \frac{dx}{2\pi} \qquad (5)$$

where

$$G(\omega) = \mathcal{F}[g(t)] \quad , \qquad (6)$$

In this case

$$G(\omega) = \int_{-T}^{T} e^{-i\omega t}\ dt \qquad (7)$$

$$G(\omega) = 2T\ \frac{\sin \omega T}{\omega T} \quad . \qquad (8)$$

Thus the computed transform can be obtained by convolving the true transform with the function $G(\omega)$; this process has the following

qualitative effects:

1. $F(\omega)$ is reproduced in frequency regions where it is substantially constant over a frequency range wide compared to $1/T$ cps (the "width" of $G(\omega)$).
2. Any variations in $F(\omega)$ which occur in a frequency range narrow compared to $1/T$ cps will be smoothed.
3. Ripples similar to those in $G(\omega)$ are introduced at discontinuities in $F(\omega)$.

These qualitative observations must be qualified by noting that if $f(t)$ happened to be zero for $t > T$ no error at all would result from the truncation. The process of convolving its transform with $G(\omega)$ would leave $F(\omega)$ unchanged.

The effect of truncation can be more appropriately treated by consideration of the portion cut off, if it is known. In the case of the impulse response of a plasma-filled waveguide, the long-time asymptotic form may be expressed simply for the compressional mode as an exponentially damped sine wave at the cutoff frequency. Suppose

$$f^*(t) = f(t) - e(t) \quad . \tag{9}$$

The Fourier transform is linear; therefore

$$F^*(\omega) = F(\omega) - E(\omega) \tag{10}$$

where $E(\omega)$ is the transform of $e(t)$. Now let $e(t)$ have the following form:

$$e(t) = A\, e^{-\alpha t} \sin(\omega_o t + \theta)\, U(t - T) \tag{11}$$

where $U(t)$ is the unit step function. This can be rewritten

$$e(t) = e_o(t - T)\, U(t - T) \tag{12}$$

where

$$e_o(t) = A_1 e^{-\alpha t} \cos \omega_o t + A_2 e^{-2t} \sin \omega_o t \tag{13}$$

$$A_1 = A\, e^{-\alpha T} \sin(\omega_o T + \theta) \tag{14}$$

and

$$A_2 = A\, e^{-\alpha T} \cos(\omega_o T + \theta) \quad . \tag{15}$$

The shifting theorem of Laplace transform theory now yields

$$\mathcal{L}\,[e(t)] = e^{-sT}\ \mathcal{L}[e_o(t)]$$

$$= \frac{e^{-sT}\,(A_1 s + A_2\,\omega_o)}{(s+\alpha)^2 + \omega_o^2} \quad . \tag{16}$$

Replacing s by $i\omega$ to obtain the Fourier transform

$$E(\omega) = \mathcal{F}[e(t)] = \frac{e^{-i\omega T}(i\omega A_1 + \omega_o A_2)}{(i\omega+\alpha)^2 + \omega_o^2} \quad . \tag{17}$$

The error transform has the magnitude

$$|E(\omega)| = \sqrt{\frac{(A_2\omega_o)^2 + (A_1\omega)^2}{(\omega_o^2 + \alpha^2 - \omega^2)^2 + (2\alpha\omega)^2}} \quad . \tag{18}$$

If the damping is slight, $\alpha \ll \omega_o$, the maximum magnitude occurs nearly at $\omega = \omega_o$ and is given by

$$|E(\omega)|_{max} \cong \frac{A\, e^{-\alpha T}}{2\alpha} \qquad \text{at} \quad \omega \approx \omega_o \quad . \tag{19}$$

It is to be noted that $A\, e^{-\alpha T}$ is the value of the envelope of $e(t)$ at the truncation point. The distribution of $E(\omega)$ with frequency depends on the relative sizes of A_1 and A_2 and is sketched in Figure A-1 for two extremes. The result given in 19 can be expressed in another way in terms of $\tau = 1/\alpha$, the time constant of the exponential envelope of $e(t)$, as

$$|E(\omega)|_{max} = \frac{\tau}{2} \cdot \begin{pmatrix}\text{envelope magnitude} \\ \text{(at truncation point)}\end{pmatrix} \quad . \tag{20}$$

B. Sampling

Let us now take for the computed transform

$$F^*(\omega) = \mathcal{F}[f(t)\, h(t)] \tag{21}$$

where

$$h(t) = \frac{2T}{2N+1} \sum_{k=-N}^{N} \delta(t - k\Delta t) \quad . \tag{22}$$

The factor $2T/(2N+1)$ is included to make the areas of $h(t)$ and $g(t)$ of the previous section equal. Again $F^*(\omega)$ can be expressed as a convolution

$$F^*(\omega) = \frac{1}{2\pi} \int_{-\infty}^{\infty} F(x)\, H(\omega - x)\, dx \tag{23}$$

where

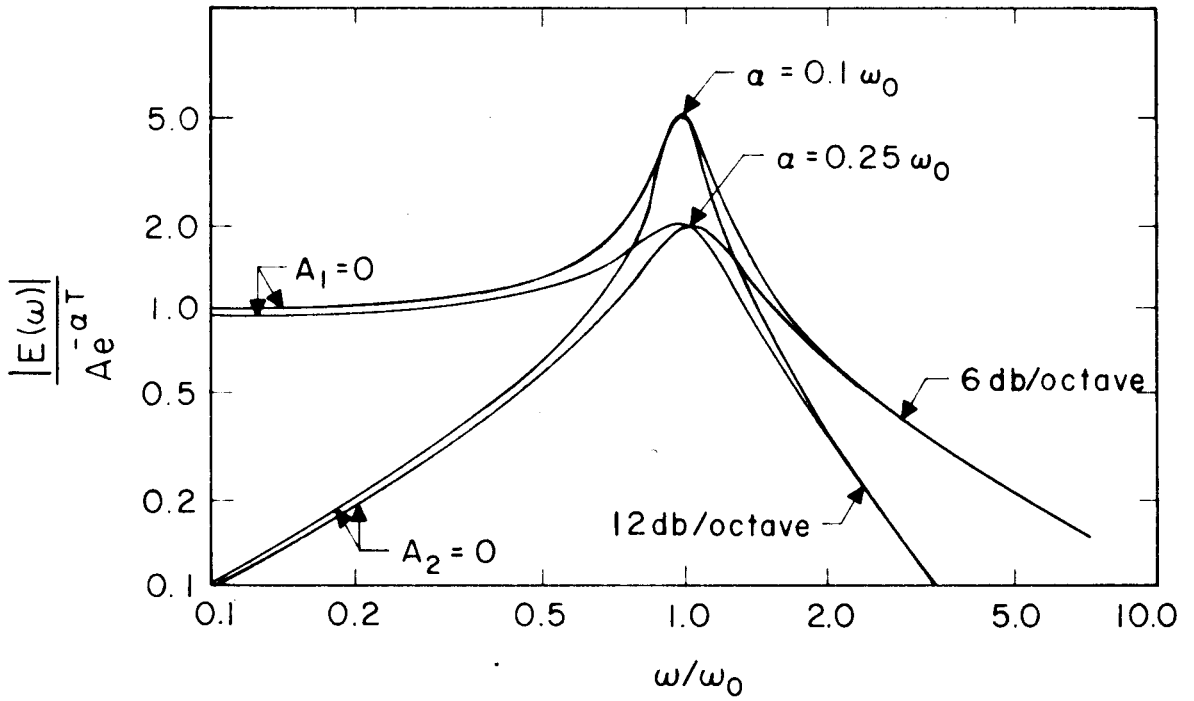

Figure A-1. Truncation Error Amplitude

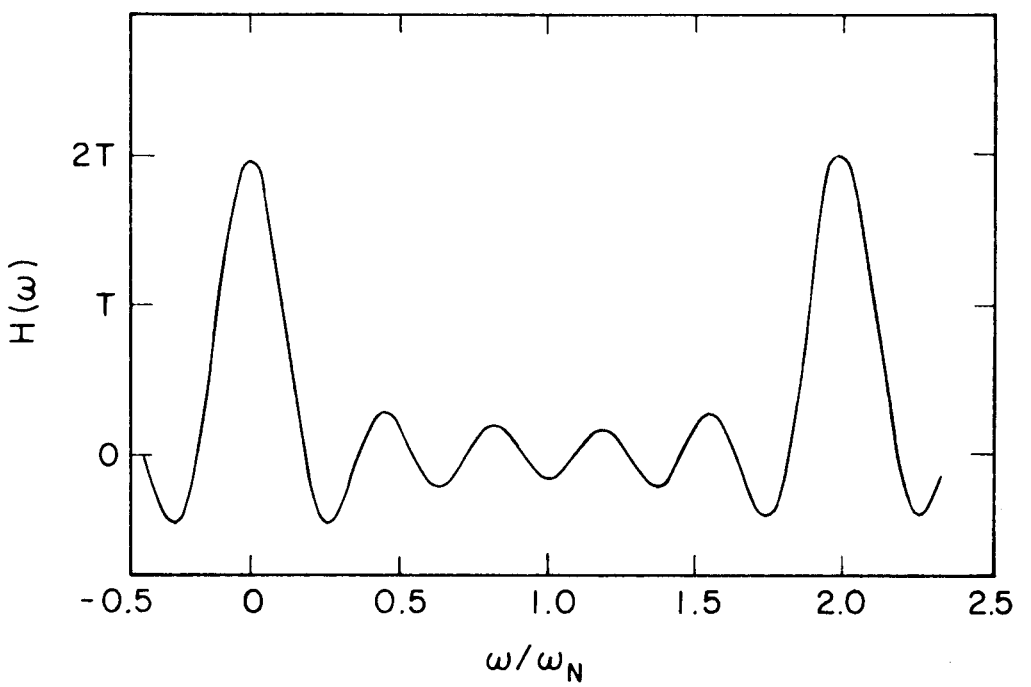

Figure A-2. Sampling Error for N = 5

$$H(\omega) = \mathcal{F}[h(t)]$$

$$= \frac{2T}{2N+1} \int_{-\infty}^{\infty} e^{-i\omega t} \sum_{k=-N}^{N} \delta(t - k\Delta t)$$

$$= \frac{2T}{2N+1} \sum_{k=-N}^{N} e^{-i\omega k\Delta t} \quad . \tag{24}$$

The sum in equation 24 can be evaluated in closed form (20)

$$H(\omega) = \frac{2T}{2N+1} \frac{\sin(\frac{2N+1}{2}\omega\Delta t)}{\sin\frac{\omega\Delta t}{2}} \quad . \tag{25}$$

This function is sketched in Figure A-2 and is seen to have large humps of height $2T$ and width $\frac{4\pi}{(2N+1)\Delta t}$ spaced at intervals of $\frac{2\pi}{\Delta t} = 2\omega_N$. The frequency $\omega_N = \pi/\Delta t$ is called the Nyquist frequency. The large humps are separated by smaller ripples decreasing in amplitude to $2T/(2N+1)$ midway between the main humps. In the vicinity of the origin, $\omega\Delta t \ll 1$, replacing the sine by its argument and approximating $\frac{2N+1}{2}$ by N yields

$$H(\omega) = 2T \frac{\sin \omega T}{\omega T} \quad , \qquad \omega\Delta t \ll 1 \, , \qquad N \gg 1 \quad . \tag{26}$$

This result is the same as $G(\omega)$, equation 8. The main effect of digitization is thus the presence of additional humps in $H(\omega)$ at even multiples of the Nyquist frequency. This becomes clearer if T is allowed to increase indefinitely with the sample time Δt fixed. This process causes the height of the main humps to increase and the width

to decrease; the area remains fixed. The subsidiary ripples remain more or less fixed in height and more numerous. In the limit

$$H(\omega) \rightarrow 2\pi \sum_{k=-\infty}^{\infty} \delta(\omega - 2k\omega_N) \tag{27}$$

as $N,T \rightarrow \infty$ with Δt fixed. Convolution of this limiting function with $F(\omega)$ has the simple result

$$F^*(\omega) \rightarrow \sum_{k=-\infty}^{\infty} F(\omega - 2k\omega_N) \quad . \tag{28}$$

It is apparent then, that the value of $F^*(\omega)$ for a given frequency will be significantly different from $F(\omega)$ if F has an appreciable value at frequencies whose magnitudes are spaced ω radians/sec above and below every even multiple of ω_N. This effect is known as aliasing. In practice, Δt should be chosen small enough so that ω_N is considerably greater than the highest frequencies at which $f(t)$ has any significant energy.

C. Additive Noise

An error in reading the value of $f(t)$ at a sample point may be taken into account by adding a noise signal $n(t)$ to the given function. Then the effect in the frequency domain is to add to $F^*(\omega)$ a noise spectrum

$$N^*(\omega) = \frac{T}{N+1} \sum_{k=0}^{N} e^{-\frac{1}{2}ik\omega\Delta t}\, n(k\Delta t) \quad . \tag{29}$$

We shall be content with finding the mean or expected value of $N^*(\omega)$ and its standard deviation. It will be assumed that the error is independent from sample to sample (white noise) and stationary (statistics independent of time). If $p(n)$ is the probability distribution function of n, the assumption of white noise permits us to write

$$p(n_i, n_j) = p(n_i)\, p(n_j) \tag{30}$$

for the joint probability distribution of $n_i = n(t_i)$ and $n_j = n(t_j)$. The mean value of $n(t)$ is assumed to be zero:

$$E[n] = \int_{-\infty}^{\infty} n\, p(n)\, dn = 0 \quad . \tag{31}$$

The mean value of the noise spectrum can now be computed.

$$\begin{aligned} E[N^*(\omega)] &= \int_{-\infty}^{\infty} N^*(\omega)\, p(n) dn \\ &= \frac{T}{N+1} \sum_{k=0}^{N} e^{-ik\omega\Delta t} \int_{-\infty}^{\infty} n(k\Delta t)\, p(n) dn \qquad (32) \\ &= 0 \quad . \end{aligned}$$

The expected value of the square of the magnitude of N^* is

$$E[|N^*(\omega)|^2] = \left(\frac{T}{N+1}\right)^2 E\left[\sum_{k=0}^{N} \sum_{j=0}^{N} e^{-i(k-j)\omega\Delta t}\, n(k\Delta t)\, n(j\Delta t) \right] \quad . \tag{33}$$

The double sum in 33 can be separated into one sum involving only the

terms for which $k \neq j$ and another involving the rest of the terms. The first yields

$$E\left[\sum_{\substack{j,k=0 \\ j \neq k}}^{N} e^{-i(k-j)\omega\Delta t}\right] n_k n_j$$

$$= \int_{n_k}\int_{n_j}\left[\sum_{\substack{j,k=0 \\ j \neq k}}^{N} e^{-i(k-j)\omega\Delta t}\, n_k n_j\right] p(n_k,n_j)\,dn_k\,dn_j \quad . \qquad (34)$$

Interchanging the sums and integrals and noting that the exponential is not involved in the integration and may be taken outside, the remaining integral is by equations 30 and 31

$$\begin{aligned}\iint p(n_k,n_j)\,dn_k\,dn_j &= \iint p(n_k)\; p(n_j)\; dn_k\,dn_j \\ &= \int p(n_k)\,dn_k \int p(n_j)\,dn_j \qquad (35) \\ &= 0 \quad .\end{aligned}$$

Thus only the terms with $j = k$ remain and

$$\begin{aligned}E[|N^*(\omega)|^2] &= \left(\frac{T}{N+1}\right)^2 E\left[\sum_{k=0}^{N} n^2(k\Delta t)\right] \\ &= \frac{\sigma_N^2\, nT^2}{N+1} \qquad (36)\end{aligned}$$

where $\sigma_N^2 = E[n^2(t)]$ is the variance of the noise signal.

D. Timing Jitter

Suppose that there is an error ϵ_k in the time t_k at which a sample is taken; then for small ϵ_k

$$f(t_k + \epsilon_k) = f(t_k) + \epsilon_k f'(t_k) \quad . \tag{37}$$

If this value is used in place of $f(t_k)$ it is equivalent to adding a noise signal

$$m(t_k) = \epsilon_k f'(t_k) \tag{38}$$

to $f(t)$ or a noise spectrum

$$M(\omega) = \frac{T}{N+1} \sum_{k=0}^{N} \epsilon_k f'(k\Delta t)\, e^{-ik\omega\Delta t} \quad . \tag{39}$$

We next find some properties of $M(\omega)$ assuming that the errors at different times are uncorrelated. Let

$$E(\epsilon_k) = 0 \tag{40}$$

$$E(\epsilon_k \epsilon_j) = \begin{cases} E(\epsilon_k)\, E(\epsilon_i) = 0 \; ; & j \neq k \\ E(\epsilon_k^2) = \sigma_\epsilon^2 \; ; & j = k \end{cases} \quad . \tag{41}$$

Following the procedure used in the last section, it can be shown that

$$E[M(\omega)] = 0 \tag{42}$$

and

$$E[|M(\omega)|^2] = \left(\frac{T}{N+1}\right)^2 \sigma_\epsilon^2 \sum_{k=0}^{N} [f'(k\Delta t)]^2 \quad . \tag{43}$$

For large N the sum in 43 is well approximated by an integral

$$\sum_{k=0}^{N} [f'(k\ \ t)]^2 = \frac{1}{\Delta t} \int_0^T [f'(t)]^2\, dt$$

$$= \frac{T}{\Delta t} [f']^2_{avg}$$

$$= N[f']^2_{avg} \quad . \tag{44}$$

Equation 43 then yields

$$E[\,|M(\omega)|^2] \cong \frac{T^2\sigma_\epsilon^2}{N} f'^2_{rms} \quad . \tag{45}$$

APPENDIX B

METHOD FOR COMPUTING WEIGHTS USED IN CURVE FITTING

We have used the estimates of the additive noise and jitter reading errors to estimate the errors in the propagation and attenuation constants in the following way.

If we represent the probable error amplitude by A_e and the measured signal transform amplitude at a particular frequency by A_s or $A_s(\omega)$, then in general the amplitude will be given by

$$A(\omega) = A_s(\omega) \pm A_e \quad . \tag{1}$$

The attenuation constant α corresponding to the amplitude A is given by

$$\alpha = -\frac{1}{z} \log \left(\frac{A}{A_o}\right) \tag{2}$$

where A_o is related to the driving pulse amplitude. The corresponding expressions for α_s and α_e are

$$\alpha_s = \frac{1}{z} \log \left(\frac{A_o}{A_s}\right) \tag{3a}$$

$$\alpha_e = \frac{1}{z} \log \left(\frac{A_o}{A_e}\right) \quad . \tag{3b}$$

Using these expressions we may solve for α in terms of α_s and α_e with the result that

$$\alpha = \alpha_s - \frac{1}{z} \log \left[1 \pm e^{(\alpha_s - \alpha_e)z}\right] \quad . \tag{4}$$

The uncertainty δ in α is then taken to be the difference between α and α_s or

$$\delta_{\pm} = \frac{1}{z} \log \left[1 \pm e^{(\alpha_s - \alpha_e)z} \right] \quad . \tag{5}$$

If the measured amplitude were smaller than the error amplitude, α_s would be greater than α_e so that the expression inside the brackets could become negative. In order to avoid the possibility of taking the logarithm of a negative number, we have arbitrarily chosen to define the uncertainty in α by the positive sign, so we use δ_+ always.

We have also assumed a probable error of approximately 5% in the determination of A_o so that we have a δ_o where

$$\delta_o = \frac{.05}{z} \tag{6}$$

which is independent of frequency.

Using these measures of our estimate of the probable errors, we have arbitrarily chosen the weight function for each frequency $W_\alpha(\omega)$ to be inversely proportional to the square root of the sum squares of $\delta_+(\omega)$ and δ_o so that

$$W_\alpha(\omega) = \frac{W_o}{\sqrt{\delta_+^2(\omega) + \delta_o^2}} \tag{7}$$

where W_o is chosen such that

$$\sum_{i=1}^{N} W_\alpha(\omega_i) = N \quad . \tag{8}$$

The weighting function for the phase information is even more

arbitrary, for it is not known how to make good estimates of the errors that should be expected in this data. However, several general considerations have been made quantitative in an arbitrary way, so that the same scheme may be used with each set of data. We first presume that the phase error will be larger where the amplitude is smaller, and we choose to assume that the error in the propagation constant β where the amplitude is largest is equal to $\pi/4z$. The error is then assumed to increase proportionally as the attenuation constant increases, and the weights are assumed inversely proportional to this error, hence

$$W_p(\omega) \propto \frac{1}{\frac{\pi}{4z} + \alpha_s(\omega) - \alpha_{minimum}} \quad . \tag{9}$$

As β increases, however, the probable error increases only as the error assumed above, so that the percentage error may get smaller if β increases faster than the denominator in equation 9. Hence we choose to weight the phase differences proportional to β so that

$$W_\beta(\omega) = \frac{W_1 \beta(\omega)}{\frac{\pi}{4z} + \alpha_s(\omega) - \alpha_{minimum}} \tag{10}$$

where W_1 is chosen such that

$$\sum_{i=1}^{N} W_\beta(\omega_i) = N/2 \quad . \tag{11}$$

It is apparent from equation 11 that the phase errors have been given

half the weight the amplitude errors received and this is due to the fact that we wish to determine ν and η primarily from the amplitude data, and suppressing the phase data has been found not to affect the determination of γ which is determined primarily from the phase information.

These expressions serve to define uniquely the weights used in the weighted average of the errors, but it can only be claimed that this scheme exhibits some of the desired characteristics. Other schemes have been tried, ranging from equal weights for the differences at all frequencies to more extreme weights near maximum amplitude or maximum phase with the result that some values of the parameters might be changed by several percent, but never greatly, so we do not believe any significant systematic errors are introduced by the scheme described above. This method does have some merit in that it does some of the things one would expect an appropriate scheme to do.

REFERENCES

1. H. Alfvén, Ark. Mat., Astr. Fysik, 29B, 1 (1962).

2. C. Walén, Ark. Mat., Astr. Fysik, 30A, No.15 (1944); 31B, No.3 (1944); 33A No.18 (1946).

3. E. Astrŏm, Ark. Fys., 2, 443 (1950); Nature 165, 1019 (1950).

4. N. Herlofson, Nature 165, 1020 (1950).

5. A. W. DeSilva, Experimental Study of Hydromagnetic Waves in Plasma, Lawrence Radiation Laboratory Report UCRL 9601 (March 1961), 96-100.

6. S. Lundquist, Phys. Rev. 76, 1805 (1949); Nature 164, 145 (1949).

7. B. Lehnert, Phys. Rev. 94, 815 (1954).

8. T. K. Allen, W. R. Baker, R. V. Pyle, and J. M. Wilcox, Phys. Rev. Letters 2, 383 (1959).

9. D. F. Jephcott, Nature 183, 1652 (1959).

10. J. M. Wilcox, F. I. Boley, and A. W. DeSilva, Phys. Fluids 3, 15 (1960).

11. T. H. Stix, Phys. Rev. 106, 1146 (1957).

12. D. G. Swanson, R. W. Gould, Bull. Am. Phys. Soc. 8, 152 (1963).

13. D. F. Jephcott, Bull. Am. Phys. Soc. 8, 152 (1963).

14. L. Spitzer, Jr., Physics of Fully Ionized Gases, Interscience Publishers Inc., New York, 1957, p.21.

15. A. G. Lieberman, private communication.

16. W. B. Kunkel, R. A. Gross, Hydromagnetic Ionizing Waves, Lawrence Radiation Laboratory Report UCRL 9612 (1961).

17. W. Cooper III, private communication.

18. A. DeSilva, op.cit., p.58.

19. I. B. Bernstein, S. K. Trehan, Nuclear Fusion 1, 3-41 (1960).

20. E. A. Guillemin, Mathematics of Circuit Analysis, Wiley, 1949, p.486.